- 1 Dynamics, predictability, impacts, and climate change considerations of the catastrophic 2 Mediterranean Storm Daniel (2023)
- 3 Emmanouil Flaounas<sup>1,2</sup>, Stavros Dafis<sup>3</sup>, Silvio Davolio<sup>4,5</sup>, Davide Faranda<sup>6, 7, 8</sup>, Christian Ferrarin<sup>9</sup>,
- 4 Katharina Hartmuth<sup>1</sup>, Assaf Hochman<sup>10</sup>, Aristeidis Koutroulis<sup>11</sup>, Samira Khodayar<sup>12</sup>, Mario Marcello
- 5 Miglietta<sup>13</sup>, Florian Pantillon<sup>14</sup>, Platon Patlakas<sup>2,15</sup>, Michael Sprenger<sup>1</sup>, Iris Thurnherr<sup>1</sup>

- 8 1. Institute for Atmospheric and Climate Science, ETH Zurich, Zurich, Switzerland
- 9 2. Institute of Oceanography, Hellenic Centre for Marine Research, Athens, Greece
- 10 3. National Observatory of Athens, Institute for Environmental Research and Sustainable
- 11 Development, I. Metaxa & Vas. Pavlou, P. Penteli (Lofos Koufou), 15236 Athens, Greece
- 12 4. Dipartimento di Scienze della Terra, Università di Milano, Milan, Italy
- 13 5. Institute of Atmospheric Sciences and Climate, National Research Council, Bologna, Italy
- 14 6. Laboratoire des Sciences du Climat et de l'Environnement, UMR 8212 CEA-CNRS-UVSQ,
- 15 Université Paris-Saclay & IPSL, CE Saclay l'Orme des Merisiers, 91191 Gif-sur-Yvette, France
- 16 7. London Mathematical Laboratory, 8 Margravine Gardens, London W6 8RH, UK
- 17 8. LMD/IPSL, ENS, Université PSL, École Polytechnique, Institut Polytechnique de Paris, Sorbonne
- 18 Université, CNRS, Paris France
- 19 9. CNR National Research Council of Italy, ISMAR Institute of Marine Sciences, Venice, Italy
- 20 10. Fredy and Nadine Herrmann Institute of Earth Sciences, Hebrew University of Jerusalem,
- 21 Edmond Safra Campus, Jerusalem, Israel
- 22 11. School of Chemical and Environmental Engineering, Technical University of Crete, 73100
- 23 Chania, Greece
- 24 12. Mediterranean Centre for Environmental Studies (CEAM), Charles R. Darwin Street, 14 46980
- 25 Paterna, Valencia (Spain)
- 26 13. Institute of Atmospheric Sciences and Climate, National Research Council, Padua, Italy
- 27 14. Laboratoire d'Aérologie, Université de Toulouse, CNRS, UPS, IRD, Toulouse, France
- 28 15. Department of Physics, National and Kapodistrian University of Athens, Athens, Greece

29 30

#### 31 Abstract

- 32 In September 2023, Storm Daniel formed in the central Mediterranean Sea—as—an intense-
- 33 Mediterranean cyclone, causing significant socioeconomic impacts in Greece, including fatalities and
- 34 severe damage to agricultural infrastructure. Within a few days, it evolved into a tropical-like storm
- 35 (medicane) that made landfall in Libya, likely becoming, to our knowledge, the most catastrophic and
- 36 lethal weather event ever documented in the region.
- 37 This study places Storm Daniel as a centerpiece of the disasters in Greece and Libya. We aim to-
- 38 conducted a comprehensive analysis that links a cyclone system with hazardous weather conditions
- 39 relevant to extreme precipitation, floods, and significant sea wave activity. In addition, we examine
- 40 Daniel's predictability in different development stages and draw connections with previous case
- 41 studies. Finally, given the extreme precipitation produced by Daniel, we place our findings in a
- 42 climatological context to better understand its implications for numerical weather prediction and
- 43 climate change attribution. Given the climatologically extreme precipitation, produced by Daniel, we
- 44 examine the capacity of numerical weather prediction models to capture such extremes and we finally
- 45 investigate potential links to climate change.
- 46 Daniel initially developed like any other intense Mediterranean cyclone, including medicanes, due to
- 47 upper tropospheric forcing followed by Rossby wave breaking. At this stage, it produced significant
- 48 socioeconomic impacts in Greece, even i.e. in areas located far from its center. As it intensified and
- 49 attained tropical-like characteristics, it developed markedly just prior to landfall, reaching peak
- 50 intensity over land. it peaked after landfall in Libya, where its socioeconomic impacts were the most-
- 51 severe. Considering short lead times (around four days), cyclone formation exhibited low
- 52 predictability, whilst landfall in Libya was more predictable. The cyclone's formation had low-
- 53 predictability even at short lead times (around four days), while the landfall in Libya was more

54 predictable within the same lead time. Our analysis of impacts highlights that numerical weather 55 prediction models can capture the extreme character of precipitation and flooding in both Greece and 56 Libya, providing crucial information on the expected severity of imminent flood events.

57 We also examine moisture sources contributing to extreme precipitation. Our findings indicate that 58 large-scale atmospheric circulation was the primary driver, but, as Daniel matured, it drawingdrew 59 drawing substantial water vapor from the eastern Mediterranean, and Black Seas and continental 60 Europelocal maritime areas within the Mediterranean. The intensification of storm Daniel was likely 61 driven by anomalously warm SST in the Mediterranean and Black Sea, enhancing evaporation and 62 contributing to the extreme precipitation along the Lybian coast. Daniel produced extreme 63 precipitation amounts in a climatological context, fueled by a warmer Mediterranean Sea and 64 atmosphere. Finally, oOur analysis supports interpreting its impacts as characteristic of human-driven 65 climate change but also highlights the exceptionality of this cyclone, especially in its medicane phase, 66 which complicates the comparison with other cyclones.

#### 67 1. Introduction

68 In early September 2023, a low-pressure system developed within the central Mediterranean Sea, 69 close to Greece. Due to the expected severity of the event, on 4 September 2023, the Hellenic 70 National Meteorological Service named the upcoming Sstorm 'Daniel'. Daniel evolved into a deep 71 cyclone within a few days and began moving erratically southward. On the 8th, it shifted eastward and 72 eventually made landfall along the coast of Libya as a powerful system (Fig. 1a). Within a few days, 73 Daniel evolved into a deep cyclone that propagated erratically southwards, then turned towards the 74 east on 8th, and then developed into a deep cyclone \$\frac{1}{2}\$

76 propagated southwards, making landfall at the coast of Libya (Fig. 1a). Daniel led to substantial, 77 unprecedented socio-economic impacts in the Central-Eastern Mediterranean from 4 to 11 September 8 2023, all attributed to the same weather system.

80 In the cyclogenesis stage, on 5 September 2023, the weather station network of the National 81 Observatory of Athens in Greece (NOAAN; Lagouvardos et al., 2017) measured more than 750 mm 82 of accumulated daily rainfall in the eastern part of the Thessaly region (flooded areas are shown in 83 cyan colours in Fig. 1b) and up to 1235 mm within four days. Thessalyhe eastern parts of Greece 84 experienced flooding (Fig. 1b) that led to 17 fatalities, the loss of 25% of Greece's annual agricultural 85 production, and the destruction of the local road network. About five days later, on 10 September 86 2023, the cyclone made landfall near Benghazi, Libya. As a result, northeastern Libya's population of 87 884,000 people has been affected directly in five governoratesprovinces by the collapse of two dams. 88 About 30% of the city of Derna was flooded (Fig. 1c), and almost 900 buildings, roads, and other 89 infrastructures were destroyed were destroyed, including roads damage and other infrastructure in the 90 area (OCHA 2023, UNICEF 2023). According to the DTM update (IOM 2023), over 5,000 people 91 were presumed dead, 3,922 deaths were registered in hospitals, 10,000 people were declared missing 92 by the Libyan government and Red Crescent Society, while at least 30,000 people were recognized as 93 internally displaced (UNICEF 2023, IOM 2023) in the Derna area. Extensive damage affected critical 94 infrastructure such as hospitals and drinking water supply systems. Many roads were rendered 95 impassable, making humanitarian aid and supplies difficultit difficult for humanitarian aid and 96 supplies. At least a \$10 million budget was allocated from the UN Central Emergency Response Fund 97 to scale up intervention in response to the Libya disaster, and almost \$72 million US dollars were 98 requested to cope with the most urgent needs of around 250,000 people (OCHA 2023) just for the first 99 three months after the flooding. 100

Daniel was an intense cyclone, Daniel was an intense cyclone, preceded by Rossby wave breaking over the Atlantic Ocean, which led to the formation of an omega blocking pattern (Couto et al., 2024) and the subsequent intrusion of an upper-level trough in the Mediterranean.preceded by Rossby wave breaking, forming an omega blocking configuration (Couto et al., 2024), and the consequent intrusion of an upper-level trough. This scenario is commonly observed before the formation of intense Mediterranean cyclones, including medicanes (Raveh-Rubin and Flaounas, 2017). From the

107 perspective of atmospheric dynamics, upper tropospheric systems are often precursors of 108 Mediterranean cyclogenesis. Such systems force ascent by advancing upper level PV 109 structures. Indeed, troughs and cut off lows correspond to stratospheric air intrusions that impose 110 significantly high potential vorticity (PV) anomalies and thus trigger baroclinic instability (Flaounas 111 et al., 2022). While the formation of Mediterranean cyclones is almost entirely dependent on 112 baroclinic instability, the development and intensification of a cyclone into a deep low-pressure 113 system is also a function of diabatic processes. More precisely, latent heat release close to the cyclone 114 centre, mainly due to convection, is a source of positive PV anomalies at low levels, eventually 115 translating into enhanced cyclonic circulation. Therefore, baroclinic instability and latent heat release 116 are the eyelone development's main forcings. Both processes drive are modulating factors of cyclones' 117 intensification from the cyclogenesis stage until maturity, i.e., when the cyclone reaches its minimum 118 pressure at the centre. A complete review of 119 Mediterranean cyclone dynamics is available by 119 Flaounas et al. (2022), while a recent thorough analysis of the interplay and synergies between 120 baroclinic and diabatic forcing of 120 o

122

123 As an environmental hazard, cyclones may produce heavy precipitation from the stage of genesis until 124 their lysis, close to their centres but also in remote areas due to localized convective cells 125 (Raveh-Rubin and Wernli, 2016), warm conveyor belts and frontal structures (Pfahl et al., 2012; 126 Flaounas et al., 2018). Regardless of whether precipitation is stratiform or convective, the large-scale 127 atmospheric circulation can considerably contributes by to essential for transporting water vapour 128 toward the Mediterranean and thus "feeding" the cyclone-induced precipitation (Flaounas et al., 2019; 129 Hochman et al., 2024). Indeed, the Mediterranean basin is composed of a relatively closed sea 130 surrounded by continental areashigh mountains. Consequently, Mediterranean cyclones have fewer 131 water sources than their counterparts over the open oceans. In these regards, large-scale ventilation of 132 water vapour from the Atlantic Ocean and other remote regions towards the Mediterranean has been 133 shown in numerous cases to enhance heavy precipitation, together with local evaporation due to 134 cyclone-induced high wind speeds (Duffourg and Ducrocq, 2011; Flaounas et al., 2019; Khodayar et 135 al., 2021; Sioni et al., 2023). Hence, identifying and quantifying the contribution of water sources to 136 heavy precipitation is a key steperucial for improving our ability to forecast socio-economic forecast 137 an events understanding socio-economic impacts in the Mediterranean (Hochman et al., 2022a; Khodayar et al., 2025). 138

139

140 From a climatological standpoint, cyclones are responsible for the weather features that lead to most 141 of the wind and precipitation extremes within the Mediterranean In a climatological context, 142 Mediterranean cyclones produce most of the wind and precipitation extremes in the region (Nissen et 143 al., 2010; Flaounas et al., 2015; Hochman et al., 2022b). Therefore, cyclones play a central role in the 144 compoundness of high-impact weather events (Catto and Dowdy, 2021; Rousseau-Rizzi et al., 2023; Portal et al., 2024), also considering that relativelyrather compact systems close to the coast 146 additionally contribute to impacts with storm surges and significantlysignificant high waves 147 considering that landfalling systems additionally produce storm surges and significant high waves 148 (Patlakas et al., 2021; Ferrarin et al., 2023a; Ferrarin et al., 2023b). Especially in the case of 149 precipitation, recent results have shown that intense water vapour transport and PV streamers, as a 150 proxy for Rossby-wave breaking, are two of the two main features that lead to extreme Mediterranean 151 events (de Vries, 2021; Hochman et al., 2023). Both of these large-scale atmospheric features favour 152 the development of cyclones into deep, low-pressure systems—: the first through baroclinic forcing and 153 the latter through diabatic forcing by intensifying convection (e.g., Davolio et al., 2020). Thus, their 154 understanding is crucial for predicting socio-economic impacts on weather and climate scales.

155

156 Future trends in cyclone-induced hazards in the Mediterranean are mainly quantified through 157 downscaling experiments (e.g., Reale et al., 2022) or statistical-deterministic methods that generate 158 synthetic tracks (e.g., Romero and Emanuel, 2017; Sandler et al., 2024). Nevertheless, additional 159 investigation is needed to assess the role of climate change in the intensification of storms that occur 160 in the current climate. While attributing extreme events, such as medicanes and high-impact 161 extratropical storms, is a rather tricky task, recent studies based on analogues have suggested that

162 several recent storms are more intense than would have been expected expected in the absence of 163 climate change (Faranda et al., 2022, 2023). Further investigation of this critical topic requires a 164 case-by-case approach to take into account the particularities of each storm and to acquire 165 a more holistic understanding of the specific processes related to cyclone intensity that are also 166 affected by climate change.

When a high-impact weather event occurs, it encompasses multiple interconnected aspects often studied separately. First, understanding the event's dynamics and physical processes is crucial for assessing and interpreting weather forecasting performance and climate change attribution. First, understanding the event's dynamics and physical processes is crucial for assessing short term forecasting and climate change implications. Second, the associated hazards—such as floods and windstorms—must be assessed according toeoneerning the specific weather conditions, as well as the vulnerability and exposure of the affected areas. This also raises questions about hazard predictability. Lastly, the event's severity must be placed within a climatological context to determine whether it produced extreme weather conditions and to attribute its intensity to climate change. Despite their interdependence, all these aspects of a specific weather event are rarely examined through an integrated approach. Our motivation is thus to apply a comprehensive framework, using Storm Daniel as the centerpiece of the September impacts in the eastern Mediterranean, and to provide an interdisciplinary assessment of the Storm Danielthe event (Shirzaei et al., 2025). In particular, we aim to address the following four questions:

- 182 1. How did cyclone development stages relate to flooding in Greece and Libya?
- How reliable and accurate were numerical models for predicting weather conditions and river discharges in relation to imminent hazards at different lead times?
- 185 3. Can numerical weather prediction models adequately simulate climate extremes?
- Can we linkattribute Storm Daniel's Daniel characteristics characteristics! to climate change?

189 The following section describes the datasets and methods, while Sectionsection 3 briefly describes the 190 storm dynamics. Section 4 analyses Storm Daniel's predictability, and Section 5 discusses the 191 potential contribution of natural variability and human-induced climate change to the characteristics 192 and evolution of Stormstorm Daniel. Section 5 is devoted to Daniel's attribution to climate change.

## 194 2. Datasets and methods

## **196 2.1 Datasets**

167

187 188

193

195

209

To analyze the evolution of the cyclone and assess its predictability, we use the operational analysis and the ensemble prediction system (EPS) products of the European Centre for Medium-Range Weather Forecasts (ECMWF). Since the last model upgrade at ECMWF (Cycle 48r1), operational analysis and medium-range ensemble forecast data have been available at a grid spacing of about 9 km. The increase in horizontal resolution and improvements in the data-assimilation system ledresulted in substantial improvements in forecast skill (ECMWF Newsletter, 176, 2023). The EPS comprises 50 members that are, initialized with a perturbed analysis using slightly modifiedaltered model physics, along with a and one control forecast. This probabilistic forecasting system has been designed to provide a range of possible weather conditions up to 15 days in advanceahead, offering providing an estimation of predictability. Finally, to assess Daniel's climatological aspects, we we were expected to provide a range of possible weather conditions up to 15 days in advanceahead, offering providing an estimation of predictability. Finally, to assess Daniel's climatological aspects, we were expected to provide a range of possible weather conditions up to 15 days in advanceahead, offering providing an estimation of predictability. Finally, to assess Daniel's climatological aspects, we were expected to provide a range of possible weather conditions up to 15 days in advanceahead, we were expected to provide a provide analysis (Hersbach et al., 2020) which provides with hourly atmospheric fields at a 208 0.25-degree grid spacing.

We used river discharge data from the Global Flood Awareness System (GloFAS; Grimaldi et al., 211 2022) to investigate the hydrological impacts of Daniel across Greece and Libya. GloFAS,—is an 212 integral component of the Copernicus Emergency Management Service (CEMS), provides focusing on 213 global operational flood forecastsing globally. It integrates the open-source LISFLOOD hydrological 214 model with ERA5 meteorological reanalysis data, interpolated to match the align—with GloFAS 215 resolution (0.05° for version 4.0), and is produced at—with a daily frequency. This dataset 216 includes encompasses historical discharge records essential forerucial—in establishing the—discharge

climatology from 1993 to 2023. To assess flood forecast potential, we also employed data from Weemployed the European Flood Awareness System (EFAS) data to assess the flood forecast potential.

The EFAS system utilises the open-source LISFLOOD hydrological model, calibrated at a higherto a
refined spatial resolution of approximately 1.5 km overat European latitudes. Forecasts are
issuedgenerated twice per dayily, based on initializedations at 00 and 12 UTC, and provide lead times
ranging extend lead times from 5 to 15 days to capture a widebroad rangespectrum of potential
weather conditions affecting impacting river discharge volumes. These forecasts incorporate data from
the 51 members of the ECMWF EPS members, the Deutsches Wetter Dienst (DWD) high-resolution
forecasts, and the 20-member COSMO Local Ensemble Prediction System (COSMO-LEPS) with 20ensemble members, ensuring a comprehensive analysis of the forecast capability potential. For this
study, we used the EFAS model forecasts driven by the 51 ensemble members of the ECMWF EPS
ensemble members.

229

230 Finally, to evaluate Daniel's marine and coastal impacts, we analyzed the wave dataresults of from the 231 Mediterranean Sea Waves Analysis and Forecast system (Korres et al., 2023), available through via the 232 Copernicus Marine Service (CMEMS). Additionally, We also determined the wave climatology was 233 derived using by analyzing the Mediterranean Sea wave reanalysis datasetavailable via CMEMS 234 (1993-2021; Korres et al., 2021), also provided by CMEMS.

235 236 2.2 Methods

237

## 238 2.2.1 Object diagnostics

239 We identify two-dimensional objects of extreme precipitation to assess the predictability of major 240 impacts in the EPS forecasts. These objects are defined separately for each member of the EPS as 241 neighbouring grid points where daily precipitation values exceed the 99th percentile in the ERA5 242 climatology (1990-2020). Using With these objects, we define the probability of of the EPS 243 forecastsing to forecast predicting extreme weather associated with due to Daniel. Similarly, we define 244 the likelihood probability of a cyclone occurrence in the EPS by identifying cyclone masks in each 245 ensemble member, based on as the outermost mean sea level pressure (MSLP) contour enclosing 246 anthat delimits a areasurface smaller than that of a circular disc with a 200 km radius of 200 km.

247

### 248 2.2.2 Air parcel trajectories and moisture source diagnostic

249 Ten-day air parcel backward trajectories wereare calculated atevery 20 hPa intervals between 1000 250 and 300 hPa from starting locations on a regular latitude-longitude grid with a 30 km, within defined 251 grid spacing within boxes over Greece and Libya (as shown in Fig. 1a), using the LAGRANTO tool 252 (Wernli and Davies, 1997; Sprenger and Wernli, 2015). We computed calculated two sets of backward 253 trajectories: (i) the first concerns Storm Daniel, withwhere trajectories initialized started every 6 hours 254 on 5 September 2023 and 11 September 2023 from the Greece and Libya boxes, respectively, using 255 the six-hourly 3D wind fields from the ECMWF operational analysis data; (ii) the second concerns air 256 parcel trajectories based on the ERA5 reanalysis wind fields and corresponds to for the 100 most 257 extreme daily precipitation events in each region of the two boxes, starting from the grid points in the 258 Greece and Libya boxes as for the first set of trajectories. These trajectories were initialized from the 259 same grid points in the Greece and Libya boxes as in the first set. These 100 extreme events were 260 identified as thethe days with the highest number of grid points within the Libya or Greece regions 261 recording experiencing daily surface precipitation exceeding the 90th percentile for autumn in (1990 -262 2023). Storm Daniel is included among the 100 most extreme daily precipitation events infor both 263 regions. Along all trajectories, wWe interpolated specific humidity, relative humidity, and the 264 boundary layer height pressure along all trajectories.

265

We identified moisture sources in Daniel and the 100 most extreme daily precipitation events using the moisture source diagnostic developed by from Sodemann et al. (2008). This method involves the tracksing of changes in specific humidity along all trajectories that precipitate upon arrival, which are defined as air parcels showing a decrease in specific humidity during the last time step before arrival and a relative humidity larger than 90% upon arrival (following Sodemann et al., 2008). Along each trajectory, an increase in specific humidity is interpreted as a moisture uptake, whileand a decrease

272 indicates specific humidity is interpreted as a moisture loss. Each moisture loss reduces the 273 contribution of preceding all previous-moisture uptakes, weighted by their magnitude of each uptake-274 amount.

275

276 For a detailed description of the moisture source diagnostic, see Sodemann et al. (2008). In our 277 analysis, The identified moisture uptakes along each trajectory were weighted by the decrease in 278 specific humidity during the last step before arrival., R and r Relative moisture uptakes were then 279 computed across over all trajectories were calculated for each six-hourly time step., Relative moisture 280 uptakes are then gridded onto a global 1° global latitude./longitude grid, and averaged for each dailyy. 281 These values relative moisture uptakes are expressed given in 10<sup>-5</sup> % km<sup>-2</sup>, indicating representing each 282 grid cell's relative contribution per km<sup>2</sup> to the precipitation in the target region. Finally, the daily 283 relative moisture sources averaged over the 100 most extreme events were are used as a 284 climatological reference for Daniel.

285

# 286 2.2.3 nalyAttribution to climate change Disentangling the role of natural variability and 287 human-driven climate change

288 We appliedused the methodology developed in the rapid attribution—framework "ClimaMeter" (see 289 Faranda et al. 2024, for more details). ClimaMeter offers a dynamic approach to contextualizing and 290 analyzing weather extremes within a climate context. This framework provides both an 291 accessible analysis—shortly after their occurrence—events.

293

In this studyparticular, we investigate analyze here how Mediterranean depressions affecting making landfalling in Greece and Libya have changed in the present climate (2001–2022; factual period) compared to howwhat they would have appeared like if they had occurred in the past climate (1979–2000; counterfactual period). To this enddo so, we compute analogues of MSLP anomalies associated withof Storm Daniel using data from the MSWX database (Beck et al., 2022). We then identify and search for significant differences between the present and past analogues in terms of MSLP pressure, near-surface temperature, precipitation, and wind speed.

301

To account for the seasonal cycle in MSLPsurface pressure and temperature—data, we remove the 303 average pressure and temperature, we remove the climatological daily mean values for each calendar 304 day at every grid point. values for eachthe corresponding calendar days at each grid point and each 305 day. Total precipitation and wind-speed data are not preprocessed. If the duration of the event is 306 longer than one day, we applyperformed a moving average across the duration ofthroughout the event 307 foron all variables. We examined all daily MSLPsurface pressure data for within each period and. We 308 selected the best 15 analogues, i.e., those thatthe data minimizeminimizing the Euclidean distance to 309 the event—itself, representing corresponding to approximately roughly the smallest 1‰ Euclidean 310 distances in each subset—of our data. We tested the extractingion of between 10 to 20 analogues and 311 found, nowithout—finding qualitatively significant variations differences in theour results. As is 312 standard in customary in attribution studies, the event itself is excluded fromor the present period 313 analysis.

314

315 Following Faranda et al. (2022), we defined several diagnostic quantities to supporting the our 316 interpretation of analogue-based attributions assignments. These quantities are then We can then 317 compared between compared these quantities between compared between the counterfactual and 318 factual periods. The quantities are:

319

320 - Analogue Quality (Q): Q is the average Euclidean distance of a given day from its 29 closest 321 analogues. If the value of Q for the extreme event belongs to the same distribution as its analogues, 322 then the event is not unprecedented, and attribution can be performed. If the Q value exceeds its 323 analogues, the event is unprecedented and not attributable.

324

325 - Predictability Index (D): Using dynamical systems theory, we can compute the local dimension D of 326 each SLP map (Faranda et al., 2017). The local dimension is a proxy for the number of active degrees

327 of freedom of the field, meaning that the higher the D, the less predictable the temporal evolution of 328 the MSLP maps will be (Faranda et al., 2017). If the dimension D of the event analyzed is higher or 329 lower than its analogues, then the extreme will be less or more predictable than the closest dynamical 330 situations identified in the data.

331

332 - Persistence Index  $(\Theta)$ : Another quantity derived from dynamical systems theory is the persistence  $\Theta$  333 of a given configuration (Faranda et al., 2017). Persistence estimates the number of days we will 334 likely observe a situation —analogous to the one under consideration.

335

336 Finally, to account for the possible influence of low-frequency modes of natural variability in 337 explaining the differences between the two periods, we also considered the potential roles of the El 338 Niño-Southern Oscillation (ENSO), the Atlantic Multidecadal Oscillation (AMO), and the Pacific 339 Decadal Oscillation (PDO). We performed this analysis using monthly indices produced by 340 NOAA/ERSSTv5. Data for ENSO and AMO were retrieved from the Royal Netherlands 341 Meteorological Institute (KNMI) Climate Explorer. At the same time, the PDO time series was 342 downloaded from the NOAA National Centers for Environmental Information (NCEI). The 343 significance of the changes between the distributions of variables during the past and present periods 344 was evaluated using a two-tailed Cramér-von Mises test at the 0.05 significance level. If the p-value is 345 smaller than 0.05, the null hypothesis that both samples are from the same distribution is rejected, 346 namely, we interpret the distributions as being significantly different. We use this test to determine the 347 role of natural variability.

348

## 349 3. Atmospheric processes leading to impacts

350

## 351 3.1 Cyclogenesis stage and impacts in Greece

352 Before Daniel formed, an omega-blocking pattern and an anticyclonic Rossby wave-breaking 353 occurred over Europe (Couto et al., 2024). Wave breaking resulted in the intrusion of an upper-level 354 PV streamer into the central Mediterranean basin, triggering cyclogenesis in the Ionian Sea on 4 355 September 2023, which eventually led to the formation of Daniel within 24 hours (marked by the 356 northernmost, first track point in Fig. 1a). Figure 2a shows that the cyclone on 65 September 2023 357 was located between Italy and Greece, developing as a moderate low-pressure system with a 358 minimum MSLP value of about 1004 hPa. The PV streamer in the upper troposphere wrapped 359 cyclonically around the cyclone centre (green contour in Fig. 2a), indicating pointing out an ongoing 360 baroclinicity which contributed to, forcing the cyclone's development. Accordingly, a high wind speed 361 pattern follows the PV streamer's orientation with larger values over the Balkans and at the northwest 362 side of the cyclone (wind barbs in Fig. 2a). This configuration summarises a typical dynamical 363 structure of Mediterranean cyclones at a stage preceding maturity, i.e., the time of maximum intensity 364 (Flaounas et al., 2015).

365

366 Accumulated precipitation also follows the typical structure of Mediterranean cyclones, with higher 367 amounts on the northeast side of the cyclone centre (Flaounas et al., 2018). Figure 2a shows that at the 368 cyclone's initial stages, the highest precipitation accumulation was observed in central Greece 369 (Dimitriou et al., 2024). The NOAAN surface stations recorded more than 750 mm of daily rainfall 370 and up to 1,235 mm within four days in the eastern parts of the Thessaly region (flooded areas are 371 shown in cyan colours in Fig. 1b). Notably these peak values are underestimated by about 40% in the 372 ECMWF analysis (with a max IFS 24-h accumulated rainfall of equal to 434 mm on 6 September 2023 373 00 UTC).

374

375 To quantify the contribution of local and remote areas to such an intense precipitation event in Greece, 376 Fig. 3a identifies the areas where moisture uptake has been significant for the air parcels that reached 377 the flooded regionarea of Thessaly (blue square in Fig. 3a), for the air parcels that reached the flooded 378 area of Thessaly (blue square in Fig. 3a), the areas where moisture uptake has been significant. 379 Considering Taking into consideration the largest moisture uptakes that contribute by at least 50% to 380 the catastrophic precipitation in Greece (dashed black contour in Fig. 3a, which that primarily 381 separates the green from the red colours), major sources were found in the Aegean and the Black Seas.

382 This tilted southwest-to-northeast orientation of essential water sources follows the pathway of strong 383 winds blowing over the Balkans and the eastern Mediterranean (wind barbs in Fig. 2a), having a 384 similar orientation astowith the upper-level PV streamer. The intense sea surface fluxes induced by 385 easterly winds are a precursor feature common towith other cyclones developing in the same area 386 (e.g., Miglietta et al., 2021). Further moisture mainly originated from central to eastern Europe and 387 the North Atlantic Ocean. These source regions generally agree<del>are in general agreement</del> with a recent study (Argüeso et al., 2024), which investigated moisture sources of rainfall over Greece from 3 to 9 September Sep 2023 using a Eulerian moisture source diagnostic. Our moisture source analysis shows larger contributions from land (54.7%) than in Argüeso et al. (2024) (27%). The Lagrangian method 391 used in our study indicates<del>shows</del> relatively large moisture contributions from the north of the Black 392 Sea because most of the air parcels arriving on 5 Sep 2023 descended and took up moisture in this 393 region before moving southwestward along the western flank of the PV streamer. The differences in 394 the land fraction between the two methods might originate from different periods used for the 395 moisture source calculations, different handling of moisture uptakes above the boundary layer, a lower 396 explained fraction of the total moisture sources (84%) with the Eulerian compared to the Lagrangian 397 diagnostic (explained fraction of 90%), and general differences in Eulerian versus Lagrangian 398 approaches. An ongoing comparison study of moisture source diagnostics investigates is investigating 399 differences in these methods in detail and will shed more light on disagreements between various 400 moisture source diagnostics. Overall, the moisture sources agree well with the climatology of 401 moisture sources of the Mediterranean cyclones that produce the heaviestmost heavy precipitation 402 events (Flaounas et al., 2019). The moisture sources shown in Fig. 3a largely overlap with the 403 climatological moisture sources of extreme precipitation in the same area. However, for Daniel, they 404 are mainly<del>mostly</del> concentrated over the Aegean Sea and regions<del>areas</del> to the northeast. In contrast, the 405 typical moisture sources for extreme precipitation in Thessaly extend further over the central 406 Mediterranean (Fig. 3b).

408 The hydrological impacts of Storm Daniel were profound and unprecedented. Figure 4 compares the 409 peak mean daily river discharge during Daniel with the historical records over three decades, 410 integrating the cumulative hydrological impacts over the entire event. Figure 4a shows the spatial 411 distribution of the maximum simulated peak discharge from January 1993 to August 2023 (i.e., before 412 Daniel), demonstrating typical peak discharge patterns in the Eastern Mediterranean. In contrast On-413 the other hand, Fig. 4b compares the event-wide mean daily peak discharge during September 2023, 414 when Daniel occurred, against the historical peak river discharges of the last 30 years in (Fig. 4a). 415 Results reveal an unprecedented magnitude of Daniel's impacts, with several areas experiencing river 416 discharges that exceeded the historical maximums by 300 to 500%. The darkest shades in Fig. 4b 417 indicate the most heavily affected regions, where the river discharge during Daniel exceeded previous 418 records by at least a factor of five, highlighting that Daniel was an unprecedented event of increased 419 river discharge levels (further discussed in section 5). At this cyclone stage, 17 human casualties were 420 registered in Thessaly, along with a profound hydrological aftermath. The extreme rainfall from 3 to 8 421 September 2023 led to widespread flooding across 1,150 km<sup>2</sup> in the Thessalian plain, 70% of which 422 was<del>constituted</del> agricultural land. The inundation severely affected the cotton crops, with floodwaters 423 covering more than 282 km<sup>2</sup>, roughly 30% of the region's total cotton fields. Over 35,000 farm 424 animals were also affected (He et al., 2023).

# 426 3.2 Mature stage and impacts in Libya

425

427 Severe weather gradually faded in Greece during the night of 6 September 2023 while the surface 428 cyclone moved southwards in phase with the upper-tropospheric low. In the following three days, 429 Daniel lingered over the central Mediterranean Sea (circular part of the track in Fig. 1a), with 430 minimum pressure remaining almost constant, close to 1004 hPa (Fig 1a). Figure 5a, b shows the sea 431 surface temperature (SST) anomaly in the area affected by Storm Daniel on 3 and 9 September, 432 respectively. Before the passage of Storm Daniel, positive SST anomalies dominated the study area, 433 with values exceeding 1°C between the Libyan coast and Greece, and lower anomalies (0 to 0.5°C) 434 observed east of Sicily. Following the storm's passage, a significant drop in SST resulted in an 435 extensive area of negative anomalies greater than 1°C between Libya and Greece. A colder SST core 436 with a decrease of less than 1.5°C was observed east of Sicily, while the northern Aegean Sea

437 experienced an even more pronounced decline. Such SST cooling after the passage of medicanes has 438 been previously diagnosed using explicitly resolved air-sea interactions in coupled atmosphere-ocean 439 models (Ricchi et al., 2017; Bouin and Lebeaupin Brossier, 2020; Varlas et al., 2020) and SST 440 observations (Avolio et al., 2024). Nevertheless, the feedback mechanism between cyclonecyclones 441 intensity and SST cooling is expected to be less important than the one typically observed in tropical 442 cyclones.

443

The role of anomalously high SSTs in intensifying cyclones has been previously shown in several studies based on numerical sensitivity experiments (Miglietta et al., 2011; Romaniello et al., 2015; Messmer et al., 2017; Pytharoulis, 2018; Argüeso et al. 2024; Sanchez et al. 2024). In the case of Daniel, deep moist convection was favoured, as suggested by the great extent of the areas covered by cold cloud-tops and intense lightning activity close to the cyclone centre (not shown). Subsequently Afterward, on 8 September, the cyclone started showing tropical-like features, like a deep warm core, spiral cloud bands, and a maximum wind speed in the low levels a few tens of km fards from the centre. Thus, the cyclone satisfies the phenomenological definition of a medicane recently proposed (Miglietta et al., submitted). Deep convection contributed to the rapid deepening of the cyclone, which reached a minimum MSLP of 997 hPa on 10 September 2023, 18 UTC, after making landfall at the northeastern coasts of Libya around 10 September 2023, 06 UTC (Fig. 1).

455

456 A comparison of Figs. 2a and 2b shows that, at the time of maturity, the area covered by at least 2
457 PVUs at 300 hPa is significantly smaller than during cyclogenesis. Nevertheless, Fig. 2b shows that
458 the 2-PVU patch is collocated with the cyclone center, advected from the west. Hewson et al. (2024)
459 proposed that this collocation is responsible for the cyclone's intensification just before landfall. TheIn460 fact, the intensification of a Mediterranean cyclone due to the synergy of upper-level baroclinic
461 forcing and deep convection is a common characteristic of intense Mediterranean cyclones, including
462 medicanes (Flaounas et al., 2021). A previous case of a medicane intensifying due to the collocation
463 of a PV streamer with the cyclone center was documented by Chaboureau et al. (2012). This
464 phenomenon reflects, on the one hand, the anomalous nature of this medicane (since medicanes
465 generally intensify over the sea and weaken inland), on the other hand, the critical role of upper-level
466 features in the evolution of Mediterranean cyclones.

467

468 At the same time, Daniel has developed a significantly stronger MSLP gradient, leading to wind 469 speeds that reaching up to 40 knots (about 20 m s<sup>-1</sup>). The intense winds associated with the storm 470 generated a severely disturbed sea in the Central Mediterranean basin, with south-westward 471 propagating waves extending from the Aegean Sea to Libya following the strong winds pathway (Fig. 472 2b). Indeed, the analysis of the wave data from the Mediterranean Sea Waves Analysis and Forecast 473 showsevinces waves with significant height of about 5 m in the Gulf of Sirte and the northern Aegean 474 Sea (Fig. 6a). Such values exceed the 99th percentile in the Mediterranean Sea wave reanalysis. A 475 peculiar aspect of Daniel is that strong winds blew in the Central Mediterranean Sea for many days. 476 As a result, Daniel preserved a severe sea state over northern Greece, in the Central Mediterranean 477 basin, and along the Libyan coast. To evaluate the cumulative impact of the event, we computed the 478 total storm wave energy (TSWE; Arena et al., 2015) by integrating the wave power contribution of 479 each sea state over the storm duration (Fig. 6b). TSWE reacheds peak values of about 3000 kWh m<sup>-1</sup> 480 in the Gulf of Sirte, which is above the 99th percentile of the total storm wave energy obtained from 481 the Mediterranean Sea wave reanalysis. Such an energetic sea condition and the storm surge affected 482 much of Libya's eastern coastal zones, causing coastal flooding, erosion, and infrastructure damage 483 (World Bank, 2023).

484

485 In terms of precipitation, Storm Daniel also presented exceptional features. During the cyclone's 486 mature stage, Bayda experienced about 414.1 mm of rainfall within less than 24 hours, equaling 80% 487 of the city's mean annual accumulated precipitation and a new daily precipitation record (Weather 488 World Meteorological Organisation, 2023a). It is worth mentioning that simulated 24-hr total 489 accumulated precipitation on 11 September 20235 in Libya, up to 382 mm, was not located within the 490 Derna catchment, as it has been discussed in Hewson et al. (2024), which was the most impacted area. 491 Significant moisture sources (red colours in Fig. 3c) encompass the cyclone centre, with more than

492 50% of the moisture originating from the Mediterranean Sea. This suggests that the cyclone-induced 493 circulation played an essential role in moistening the atmosphere within the proximity of the cyclone. 494 Nevertheless, the largest moisture sources that contribute collectivelytogether to at least 50% of the 495 total precipitation in Libya (black dashed contour encompassing green to red colours in Fig. 3c) still 496 retain a southwest-to-northeast orientation as in Fig. 3a (i.e., during the precipitation event in Greece). 497 Comparing the moisture sources betweenamong the two precipitation events in Greece and Libya, the 498 cyclone tends to attract more moisture from its surrounding area in the latter case. In contrast, in both 499 cases, northern moisture sources tend to align with the large-scale circulation responsible for 500 downstream cyclogenesis in the Mediterranean. This southwest-northeast orientation of moisture 501 sources contrasts with the climatological sources in Figs. 3b and 3d which mainly highlight, mainly 502 highlighting the importance of local sources, especially from the Mediterranean Sea westwards of the 503 two study regions.

505 Figure 4 highlights the region's exceptional river discharges, as in Greece's case exceptional river 506 discharges in the region, as in the case of Greece. However, the absence of similarly strong discharge signals in several severely impacted regions, such as the wider Pelion area in Greece and Derna 508 (Libya), is notable and can be attributed to several factors. First, the GloFAS model has limitations in 509 spatial resolution and calibration. The model operates at a resolution of approximately 5 km (0.05°), 510 which, while adequate for global-scale flood awareness, is insufficient for resolving localized 511 hydrological dynamics. For instance, the catchments east of Volos, including the wider Pelion area, 512 are approximately 30 km<sup>2</sup>, while the Derna basin spans around 575 km<sup>2</sup>. In both cases, localized 513 rainfall-runoff dynamics are critical in shaping discharge patterns, particularly during extreme events. 514 Due to insufficient in-situ discharge data, the absence of Greece and Libya in the GloFAS calibration 515 dataset further exacerbates these limitations since the model relies on generalized parameter 516 regionalization rather than site-specific calibration, introducing significant uncertainties into discharge 517 predictions. Furthermore, inaccuracies in the rainfall inputs depicted in Figure 2 propagate into the 518 discharge simulations shown in Figure 4. For instance, within the Peneus catchment, the maximum 519 recorded 24-hour accumulated precipitation was 274 mm at Zappeio and 226 mm at Neraida stations, 520 as Dimitriou et al. (2024) reported, while accumulations of up to 750 mm were recorded outside the 521 catchment, specifically over the Pelion area, east of Volos. In the Wadi Derna catchment, extreme 522 rainfall exceeded 400 mm day<sup>-1</sup>, with torrential rainfall ranging between 150 and 240 mm across 523 several locations and Al-Bayda recording a maximum of 414.1 mm (World Meteorological 524 Organisation WMO, 2023b). These rainfall extremes were underrepresented in the GloFAS rainfall 525 inputs, propagating into the discharge simulations and contributing to the muted signals observed in 526 Figure 4(b).

#### 528 4. Weather forecasting of Daniel and implications for impacts

Daniel's impacts took place in two distinct periods: during cyclogenesis and at maturity. In the former stage, most precipitation was produced in areas far from the cyclone centre, drawing moisture from the surrounding areas. At the later stage, the cyclone impacts were relevant toaround landfall, and precipitation and sea level rise were significant important close to the cyclone centre. Therefore, the two distinct stages of Daniel that provoked substantial impacts in Greece and Libya were linked to cyclone stages of different dynamics, which also have further implications for Daniel's numerical prediction. In the case of Greece, i.e., at the initial stage of Daniel, it is the timely prediction of cyclogenesis that would have primarily provided useful information to civil protection, whereas, in the case of Libya, it would have been the accurate prediction of the cyclone track, intensification, and its landfall location. This section focuses on the predictability of the environmental hazards linked to Daniel's socio-economic impacts, i.e., precipitation amounts, sea state, and cyclone track.

### 542 4.1 Forecasting the cyclogenesis stage

504

527

541

543 Concerning the cyclogenesis stage, a forecast model has to predict the formation of the cyclone to 544 provide valuable information regarding its impact. This suggests that numerical weather prediction 545 models should accurately reproduce the large-scale atmospheric circulation, the Rossby wave 546 breaking, and the consequent intrusion of the PV streamer within the Mediterranean, as shown in Fig.

547 2a by the green contour. Such a large-scale circulation pattern is absent from forecasts initialised one 548 week ahead (Fig. 7a). At a lead time of 120 hours, the PV streamer is present, though its location 549 shows high uncertainty among EPS members but with high uncertainty among the EPS members on 550 its location (Fig. 7c). Indeed, the PV distribution of all EPS members at 300 hPa (outlined by coloured 551 crosses in Fig. 7) depicts a much larger area of possible high PV values than the one in Fig. 2a. This is 552 due to the limited agreement on the occurrence -or colocation- of the intrusion of the PV streamer 553 among the EPS members, ranging between of the order of 25 to 50%, as suggested by the blue crosses 554 in Fig. 7c.

555

567

Following the uncertainty in the PV streamer occurrence, the cyclone is also absent from the MSLP ensemble average one week ahead (black contour in Fig. 7a). The MSLP spread seems and the MSLP spread seems rather consistent within the shown domain (about 1 to 3 hPa). At subsequent lead times, bigher spread of MSLP tends to concentrate close to the cyclone centre (Figs. 7c and 7e) until it becomes negligible 24 hours before cyclogenesis (Fig. 7g). At such a short lead time, the cyclone formation was forecast with confidence to occur in the Ionian Sea, to the southwest of Greece (black contours in Fig. 7g). Confident forecasts of cyclogenesis should go hand in hand with higher agreement among the EPS members on the location of the PV streamer. Indeed, 24 hours before cyclogenesis, more than 95% of EPS members agreed on the area of PV streamer intrusion. Accordingly, average values (blue contour in Fig. 7g) better match the ones in the ECMWF analysis (green contour in Fig. 2a).

To get deeper insights into the representation of cyclogenesis among the EPS members, Fig. 8 shows the level of agreement on the cyclone objects (as presented in section 2.2.1). At a lead time of 168 hours, cyclogenesis forecast was relativelyrather poor (Fig. 8a). Still, at, but at a lead time of 120 hours (Fig. 8c), cyclone centres are present (red dots in Fig. 8), scattered in the central Mediterranean but still close to the actual location where the cyclone initially formed. Higher overlapping of cyclone objects among the EPS members (green shading in Fig. 8) is indeed within the limits of the observed cyclone object, as in the ECMWF analysis (black contour in Fig. 8c). In fact, about 30% of the different EPS members produce overlapping cyclone objects. At a forecast lead time of three days, the overlapping of cyclone objects increases clearly (comparing green shaded areas between Figs 8c and strong suggesting higher agreement among the EPS members on the cyclone occurrence within the correct location. The high agreement is retained evenalso for shorter lead times (Fig. 8g).

The similar behaviour in the cyclone and PV streamer predictability relies on the direct relationship between the Rossby wave breaking over the Atlantic Ocean and the accurate prediction of Mediterranean cyclogenesis. This has been highlighted by Chaboureau et al. (2012) and Pantillon et al. (2013) for the case of the extratropical transition of a hurricane upstream of a medicane, more recently by Portmann et al. (2020) for another case, and has been demonstrated by Sherrmann et al. (2023) in a semi-idealized framework. In the case of Daniel, Hewson et al. (2024) similarly suggested the role of the extratropical transition of Hurricane Franklin as responsible for the high uncertainty one week ahead. Only in forecasts initialized after the extratropical transition has occurred is the PV streamer predicted to intrude on the Mediterranean, thus explaining the contrast between 5 and 7 days lead times. A similar "jump" in the predictability of cyclone occurrence has been shown for several medicane cases by Di Muzio et al. (2019). Most probably, this "jump" is due to the dependence of Mediterranean cyclogenesis on the preceding Rossby wave breaking and, consequently, on the credible inclusion of this event within the forecast initial conditions.

# 594 4.2 Forecasting cyclone location and intensity at the mature stage

595 Figure 1a shows that on 10 September, Daniel made landfall on the coasts of Libya. For all different 596 forecast lead times of this event, the spread of MSLP consistently retains high values close to the 597 landfalling area (right column of panels in Fig. 7). This is directly relevant to the high MSLP 598 gradients close to the cyclone centre (Fig. 2b) where even "small" negligible displacement of cyclone 599 centres may result in a relatively large standard deviation of MSLP in the EPS. Indeed, Figs. 8b and 600 8d point to the high certainty of the cyclone occurrence in the EPS, where most members produce 601 consistent and overlapping cyclone objects (depicted by dark green shading). Such performance

602 comes in contrast to forecasting the stage of cyclogenesis, where MSLP spread does not have a clear 603 pattern (the left panels of Fig. 7, green and yellow areas), and cyclone objects present limited 604 overlapping for the same lead times (e.g., comparing Figs. 8c and 8d). The limited agreement among 605 the EPS members on the PV streamer intrusion leads to considerable differences among the EPS 606 members on the location or even the occurrence of cyclogenesis. In contrast, the predictability of 607 landfall in Libya seems more consistent among the EPS members of ECMWF.

608

609 Considering a forecast lead time of 120 hours (i.e., initialization on 6 September), the cyclone has 610 already formed and was located over the central Mediterranean (just before the spiral part of the 611 track). Therefore, the cyclone has already been inscribed in the model's initial conditions. Still, from 612 the perspective of impacts, the location of landfall and the cyclone's intensity are crucial. Figure 9a 613 shows that even for an early lead time of five days (initial conditions of 5 September 2023, 0000 614 UTC), the cyclone tracks from all EPS members make landfall on the Libyan coasts. The spread of the 615 tracks is wide enough to include the actual cyclone track (in blue colour in Fig. 9a); therefore, the 616 forecast may lead to a reliable and timely warning of potential impacts.

617

Nevertheless, Fig. 9b shows that almost all the EPS members underestimated the cyclone's intensity by forecasting too high MSLP values on 10 September at the time of landfall. The intensity of the cyclone is dependent on the baroclinic and diabatic forcing of its development (Flaounas et al., 2021). Therefore, the performance of all EPS members depends on the accurate representation of the parametrized processes, mainly convection close to the cyclone centre and surface fluxes, and the morphology of the PV streamer intrusion. For the present case, Hewson et al. (2024) noted that, while in the development stage the latent heat released from convection, favoured by the high SST and intense sea surface fluxes, balanced out the tendency for frictional decay, in the last stage a marked upper-level low moving from the west (marked by high PV values in Fig. 7h) was responsible for a further deepening. Upper tropospheric forcing is crucial in accurately predicting cyclone intensity in further deepening. Upper tropospheric forcing is crucial in accurately predicting cyclone intensity in this context. While Fig. 7b —unlike Fig. 7a— shows that some EPS members align with the location of this upper tropospheric feature (blue crosses), an average of 2 PVU and an agreement above 50% among the EPS members near the cyclone center is only evident at a lead time of approximately three days (Fig. 7f, depicted by green crosses).

632

## 633 5. Daniel's impacts in a climatological context

634

## **635 5.1** Forecasting climate extremes

636 The previous sections focused on the capacity of the EPS to forecast Daniel's Daniel cyclogenesis as 637 the primary driver of impacts. In this section, we extend this analysis by focusing on the predictability 638 of hazards in a climatological context, namely extreme precipitation and consequent floods. We used 639 the ERA5 reanalysis to diagnose extremes since this product offers a reliable and consistent 640 representation of present-day climate (Hersbach et al., 2020). In this respect, the left column of Fig. 10 641 shows the area affected by extreme daily precipitation on 5 September (in red contour, explained in 642 Section 2.2.1). In addition, Fig. 10 shows the percentage of the EPS members that forecast daily 643 precipitation exceeding the climatological threshold for extremes, defined by the 99th percentile of 644 daily precipitation in ERA5 (in blue shading). At a lead time of 120 hours (Fig. 10c), less than half of 645 the ensemble members predicted the climatological extreme precipitation amounts within the area 646 delimited by the climatological values of ERA5 (red contours). Nevertheless, the area formed by the 647 blue shading in Fig. 10c is consistent with the climatological extremes. The It seems that the members 648 of the EPS that produce extreme precipitation could provide information —on the potential occurrence 649 of high-impact weather at least five days in advance. Therefore, accurately forecasting the time and 650 location of cyclone formation (as shown in Fig. 8) may play a secondary role in predicting its impacts 651 in Greece. In this context, the reliable simulation of moisture inflow, —which isappears to be more 652 closely linked to large-scale circulation, as previously discussed —by the EPS members, could be 653 more crucial for impact prediction.

654

655 Interestingly, the overlap of extreme precipitation objects among the EPS members might exceed 70% 656 in the area of Thessaly in Greece for a lead time of even 120 hours (Fig. 10c). This percentage is

657 significantly higher than the maximum percentage of overlap between the cyclone objects (Fig. 8c). 658 This suggests that the EPS members have been more consistent in the production of extreme 659 precipitation even if cyclone centres presented a comparably greater spread. For subsequent lead 660 times, the predictability of extreme precipitation strongly increases, showing a high probability for a 661 lead time of 72 hours. Indeed, almost all members predict extreme precipitation off the coast and in 662 the northeastern part of Greece within the eventually flooded area of Thessaly.

663

664 When Daniel made landfall and produced impacts on the Libyan coasts, the EPS showed higher 665 predictability, with cyclone objects and associated extreme precipitation being predicted at least five 666 days in advance by several EPS members (Fig. 10d), albeit the location of both cyclone and 667 precipitation objects are still displaced to the southwest compared to the analysis (Figs. 8d and 10d). 668 This comes perin accordance with the southern displacement of several ensemble member tracks in 669 Fig. 9a. The probability strongly increases at shorter lead times (Figs. 10f and 10h), mostly and all 670 EPS members tend to converge to similar cyclone locations when reaching a lead time of one day 671 (Fig. 8h).

672

The potential of extreme precipitation leading to substantial socio-economic impacts has also been transferred to hydrologic discharge forecasts. The hydrographs presented in Fig. 11 examine river discharge predictability as forecast by the operational European Flood Awareness System (EFAS) during Daniel. For the Peneus River outlet in Thessaly, the forecast initiated on 1 September underpredicted the peak discharge on 5 September. Nevertheless, extreme river discharges were evident for several members five days in advance. The forecast accuracy improved, getting closer to free event, with ensemble members (grey stripes) converging towards the peak discharge ("perfect forecast" - red line). This trend indicates an increasing reliability of the forecast as the lead time decreases, particularly within 48 hours of the event. The skill in discharge predictability for the River can be attributed, in part, to the large size of the basin (11.063 km²), which aligns relatively well with the spatial resolution of the EFAS model, enabling an accurate representation of distributed hydrological processes and moderating runoff variability.

685

686 The forecasts for the Wadi Derna River outlet (Fig. 11, right panels) exhibit significant variability and fail to converge during the earlier forecast initialization dates and well as at shorter lead times. This 688 persistent lack of convergence can be attributed to distinct challenges of both temporal scales. For 689 earlier forecast initialization dates, the primary source of variability lies in the westward displacement 690 of extreme precipitation predicted by the EPS (Figs. 10b and 10d). For example, forecasts initialized 691 on 9 September, during a critical period for implementing preventative measures, display a wide 692 spread and a shortfall in the median forecast compared to the benchmark (red line). This variability 693 persists even for forecasts initialized on 10 September. The failure to converge at shorter lead times is 694 compounded by challenges inherent to the Wadi Derna catchment. The resolution of the precipitation 695 forcings used in the forecasts, combined with the relatively small size (575 km²) and flash-flood-prone 696 nature of this basin, amplify the uncertainties in predicting discharge, particularly in response to 697 localized extreme rainfall.

598

Figure 4 provides critical context by comparing the peak mean daily river discharge during Storm Daniel with the historical baseline. The unprecedented magnitude of the event is evident in Fig. 4b, where river discharges exceeded the historical reanalysis by at least fivefold in certain regions. However, the relatively weak signal for the Wadi Derna catchment underscores the limitations of the GloFAS and EFAS systems in accurately resolving runoff dynamics in smaller basins. This discrepancy is primarily attributed to insufficient model resolution, inaccuracies in rainfall inputs, and the lack of detailed hydrological calibration for these catchments. In contrast, the much stronger signal observed in the Peneus catchment aligns with larger basin sizes and better-resolved hydrological roof processes, where models more effectively captured the extreme nature of the event.

708

709 The ability of EFAS to predict extreme events, as shown in Fig. 11, highlights its value in forecasting 710 severe hydrological impacts. However, discrepancies in simulated peak discharge remain apparent, 711 such as the overestimation of runoff for the Peneus River outlet. EFAS simulated peak discharge at

approximately 5000 m³ s⁻¹, whereas observed values, based on station-level data and H-Q curve estimates, were less than 2000 m³ s⁻¹ (Dimitriou et al, 2024). This overestimation reflects inherent limitations in the model's spatial resolution and hydrological representation. Furthermore, the absence of flood protection infrastructure, such as levees or dams that attenuate runoff and peak flows, is not accounted for in the EFAS and GloFAS systems, contributing to these discrepancies. Additionally, the simplified representation of retention processes, including floodplain storage and wetland buffering, further amplifies discharge estimates in some regions. For smaller basins such as Wadi Derna, the rapid hydrological response to localized extreme rainfall presents additional challenges. The variability in rainfall distribution, coupled with the model's limited ability to capture localized hydrological dynamics, results in a weaker signal for the catchment, even during an event as extreme rainfall precipitation forcings, and better calibration tailored to local catchment characteristics.

724

725 Nonetheless, EFAS's abilitythe ability of EFAS to predict extreme river discharges, particularly within 726 short lead times, demonstrates the potential of operational forecast systems in capturing the extreme 727 values of such events. Supported by EFAS and GloFAS, the Copernicus Emergency Management 728 Service (CEMS) provides critical insights into the timing and magnitude of extreme hydrological 729 events. These forecasts are vital for enhancing preparedness and response strategies in the face of 730 escalating climate extremes, offering essential tools for civil protection efforts and mitigating the 731 socio-economic impacts of such disasters.

732

# 733 **5.2** Attribution to Detecting changes in Danielselimate change The Role of Natural Variability 734 and human-driven climate change in changing Daniel's dynamics

735 We useassess Daniel's attribution to climate change using ClimaMeter's analogue-based approach (Faranda et al., 2024) to study the influence on the storm of human-driven climate change and natural 737 variability on Storm Daniel. By comparing surface pressure patterns in the periods 1979–2000 738 ("past") and 2001–present ("current"), we identify how similar Mediterranean depressions have 739 evolved. We use MSWX data to analyze temperature, precipitation, and wind speed changes changes in temperature, precipitation, and wind speed associated with these analogues, attributing observed 741 shifts to anthropogenic climate change. We repeat the analysis twice, once for 5-6 September, when 742 Daniel impacted Greece, and once for 10-11 September, when Daniel impacted Libya.

743

744 Regarding the impacts in Greece, we searched for About impacts in Greece, we search analogues for 5 745 September 2023 within the region defined within the domain shown in Fig. 12a and within the 746 extended autumn season from September to December (SOND). Figure 12a-d shows that cyclone 747 systems similar to Daniel impacting Greece have the same order of pressure minima in their centre as 748 about the same order of pressure minima in their centre as they did in the past. Figure 12e-h shows 749 that during depressions, temperatures in the Ionian Sea have increased by approximately 2°C and 750 decreased over Anatoliatemperature during depressions has increased in the Ionian Sea by about 2°C 751 and decreased over Anatolia. Precipitation analysis (Fig. 12j-l) indicates that such events produce 752 heavier rainfallshows that similar events produce heavier precipitation over the Ionian Sea and 753 Albania but generally reducedlower precipitation amounts over continental Greece and the 754 Peloponnese (ranging between 4 and 12 mm day-1). To examine potential changes in the dynamical 755 characteristics of these events, the metrics Q, D, and  $\Theta$  are computed and shown in Figs. 12q-s. The 756 metrics Q, D, and Θ (Figs 12q-s) are computed to discuss changes in the possible dynamical-757 properties of the eventeventTo. These figures reveal no significant differences between the past and 758 present climate periods. Figs 12q s show no significant changes between the two periods (present and 759 past climate). However, metric Q provides insight into the similarity of current events with past 760 analogues, showing that the events have comparable counterparts in both time frames. We can, 761 however, infer how close the event is to its analogues using the metric Q, which further highlights that-762 the event has similar analogues in past and present periods. Notably, We also find that similar events 763 have become more frequent in December, whereasile they were previously concentrated occurred 764 mainly in October (Fig. 12t). To assess the potential influence of low-frequency modes of natural 765 variability on the differences observed in the analogue composite maps, we compare the distributions 766 of ENSO, AMO and PDO values on the analogue dates in both the past and present periods and test

the statistical significance of the observed differences. To evaluate the possible role of low-frequency modes of natural variability in explaining the differences between the composite maps of analogues in the two periods, we compare the distributions of the ENSO, AMO, and PDO values on the dates of the analogues in the past and present periods, and we test the statistical significance of the observed differences. For this date, our analysis suggests that natural climate variability, particularly the AMO and PDO, may have influenced the development of the MSLP pattern associated with the storm (Figs. 12u-w). To clarify the trend in eventthe frequency of these events, Fig. 12x expands considers in each period the analysis to include 30 analogues per period instead of 15 in each period, showing an increase in their number.

776

796

811

777 We repeat the analysis for 10-11 September 2023 within the region depicted in Fig. 13a, focusing on 778 analogue detection for the SOND period. and search for analogues for SOND. Results are reported in 779 Fig. 13. The MSLP changes (Fig. 13d) show no substantial differences in the areas significantly 780 affected. The temperature changes (Fig. 13h) indicate warming of up to +2°C over the eastern part of 781 the domain. reach +2°C warmer temperatures on the east part of the domain. Precipitation changes 782 (Fig. 13l) showindicate that similar events produced higher precipitation amounts along the eastern 783 Libyan coast (ranging frombetween 5 and 9 mm day<sup>-1</sup>), which experienced intense rainfall from 784 Daniel on 10 September 2023. The metrics Q, D, and  $\Theta$  (Figs. 13q-s) show no significant differences 785 between the past and present periodstwo periods. Whereas the 5 September analysis of Q identified 786 suitable analogues, in this case, Q shows that no good analogues are available, While the 5 September-787 analysis of Q identified suitable analogues, here, Q indicates that no good analogues are available, 788 underscoring the exceptional nature of Daniel's pressure pattern when the storm impacted Libya. The 789 frequency of such events has decreased in September and November, with a slight increase observed 790 in December (Fig. 13t). Events have become less frequent in September and November and slightly 791 more common in December (Fig. 13t). As with the for 5 September, the we find that AMO and PDO 792 may have influenced the development of the MSLP pattern linked to associated with the storm (Figs. 793 13uU-w). Figure 13x showed changes in eventthe frequency of these events when 30 analogues were 794 considered<del>searched</del> for the entire period analyzed, instead of 15 in both periods. As in the case of 795 impacts in Greece, a significant increasing trend in frequency is found.

The analogues method helps us understandunderstanding extreme weather events like Daniel by comparing them to similar past events and seeing how they have changed over time. Our results suggestsugges a role of the AMO and PDO; in modulating the large-scale atmospheric patterns conducive to the development of Stormstorm Daniel. Previous studies (see Hodgkins et al. 2017 and network to the development of Stormstorm Daniel. Previous studies (see Hodgkins et al. 2017 and network to the development of Stormstorm Daniel. Previous studies (see Hodgkins et al. 2017 and network to the development of Stormstorm Daniel. Previous studies (see Hodgkins et al. 2017 and network to the jet stream across the Northern Hemisphere. Inked to alterations in the waveguide structure of the jet stream across the Northern Hemisphere. These teleconnections may precondition the synoptic environment in which Mediterranean cyclones form and evolve, as Maslova et al. (2017) suggested as suggested by Maslova et al. (2017). Thise allows us to assess whether climate change has influenced the storm's characteristics. While large-scale climate variability modes such as ENSO, AMO, and PDO can influence atmospheric conditions, our analysis does not establish a direct causal link between these modes and the development of Daniel; instead, Thisthis assessment is exploratory, highlighting potential associations without making definitive attributions given the limitations of a 40-year dataset.

812 For 5 September, when Daniel impacted Greece, we found similar past Mediterranean storms, 813 suggesting that this part of the storm's track was unusual but not unprecedented. Since we see no 814 major changes in the MSLP pattern, the increase in precipitation over the region is most likely linked 815 to higher SSTssea surface temperatures (SSTs), which provide more moisture to the atmosphere. This 816 matches other studies that show Greece experienced extremeparticularly strong moisture anomalies.

818 For 10-11 September, when Daniel reached Libya, our method found no suitable past matches, 819 highlighting the exceptional nature of the storm's pressure pattern at this stage. However, like in 820 Greece, we do not see substantial changes in MSLP., meaning—The increasedinerease in the frequency 821 of circulation analogues to Stormstorm Daniel in recent decades suggests that the synoptic conditions

822 conducive to such extreme Mediterranean cyclones are becoming more common. This shift implies a 823 heightened background risk for the occurrence of similar high-impact events under present-day 824 climate conditions. Combining multiple lines of evidence, as customary in attribution studies, we can 825 deduce that deducethat the increase in rainfall over Libya was also likely driven by warmer SSTs and a 826 warmer atmosphere, which can hold more water (Clausius-Clapeyron relationship) rather than a shift 827 in atmospheric dynamics patterns. The MSWX dataset provides a reliable representation of large-scale 828 atmospheric patterns but does not fully capture localized extreme precipitation intensities, which 829 explains why our figures underestimate the observed rainfall totals, particularly in Libya; therefore, 830 our analysis should be interpreted as reflecting broader climatological trends rather than exact 831 station-level extremes. We also acknowledge that the small-scale, Medicane-like structure of storm 832 Daniel presents significant challenges for attribution studies based on relatively coarse-resolution 833 reanalyses. In this study, we do not attempt to reproduce the mesoscale features or rapid 834 intensification processes that characterized Daniel. Instead, our analysis focuses on the large-scale 835 circulation patterns that may create a favorable environment for developing the development of such 836 compact systems. While this approach provides insights into the changing likelihood of conducive 837 synoptic configurations under current climate conditions, it is important to note that critical aspects of 838 Daniel's intensity and structure may be underrepresented in our framework. As such, our results 839 should be interpreted as exploratory and limited by the resolution and scope of the datasets employed. 840 Importantly, while Daniel brought heavy rainfall, the disaster in Derna was mainly caused by the 841 failure of poorly maintained dams (Shirzaei et al., 2025). Dente et al. (2024) confirm this, showing 842 that while rainfall was intense, it was not so extreme to explain the scale of destruction—factors like 843 unsafe building locations and poor emergency response played a major role. These considerations 844 underscore a key point: while climate change can amplify precipitation by increasing SSTs, the most 845 severe impacts often depend on societal factors such as infrastructure resilience and disaster 846 preparedness.

## 848 6. Summary and conclusions

847

859

In the last decade, more than 410,000 deaths have been attributed to weather-related disasters, mostly in low-income countries where heatwaves and intense precipitation events are the leading causes of death. Besides fatalities Aside from human casualties, 1.7 billion people have been affected in the 2010-2020 decade by these kinds of phenomena. The IFRC World Disasters Report (2020) concluded that climate change is a risk multiplier, i.e., intensifying existing vulnerabilities, particularly in low-income countries The IFRC World Disasters Report (2020) concluded that the climate acts as a risk multiplier, especially in the case of low income countries and at a regional level therein. A glaring example of the impact of such disasters has been highlighted by is are the recent floods in the Mediterranean, especially in Greece and Libya, following the Mediterranean cyclone Daniel.

This study aimed to comprehensively analyze Medicanemedicane Daniel, by linkingwhich links atmospheric dynamics, predictability, and impacts. Beyond the description of the underlying physical processes, atmospheric dynamics are used here to understand the performance of numerical weather prediction models. Impacts, in terms of floods and relevant to sea state (for Libya), have also been analyzed using concerning numerical weather prediction models. Our analysis has been framed by the climatological context of cyclone-induced precipitation and relevant impacts that link with climate change attribution of both catastrophic events. Impacts—including flooding and coastal sea-state conditions in Libya—were also evaluated with numerical weather prediction models. We placed these findings in a broader climatological context of cyclone-driven precipitation, underscoring how the observed impacts connect to climate-change attribution for both catastrophic events.

From the perspective of atmospheric dynamics, the processes governing Daniel's development—were similar to those identified for other intense Mediterranean cyclones: cyclogenesis was triggered by the intrusion of an upper-level PV streamer in the Ionian Sea, and thereafter, the cyclone propagated erratically southwards, then turned towards the east on 8 September, and then developed into a deep storm, that propagated southwards and towards Libya while it was turning into a well defined mesoscale tropical-like cyclonic system. Regarding impacts, we identified

two well-distinct stages: the first is relevant to cyclogenesis, where Daniel hadwas newly formed and affected Greece with severe floods (on 5 September 2023). In the second stage, Daniel reached maturity afterwhile making landfall in Libya, where it inflicted severe socio-economic impacts on 110 September 2023 due to floods (about 5 days after the floods in Greece). Storm Daniel produced extreme precipitation during both stages During both stages, Storm Daniel produced extreme precipitation by transporting moist air toward the flood-affected regions. The moisture transport followed the large-scale atmospheric circulation and drew on two primarymain sources: an anomalously warm Mediterranean Sea and the continental areas of central and eastern Europe. Together, these reservoirs supplied the water vapor that fueled the catastrophic rainfall. Daniel produced extreme precipitation in both stages, driving a moisture flow towards the areas that experienced the floods. The moisture transport followed the large-scale atmospheric circulation with large amounts of moisture that contributed to the catastrophic precipitation in the flooded areas were drawn locally from the Mediterranean Sea, which has been anomalously warm, but also from the continental regions of central and eastern Europe.

In Greece, the floods occurred during the cyclogenesis stage stage of cyclogenesis, in regions that were quite remote from elatively remotely from the cyclone centre. On the other hand, floods in Libya occurred close to the cyclone centre and close to at the stage of its maximum intensity. Therefore, the implication of different cyclone dynamics is important in predicting socio-economic impacts at both weather and climate scales. During its first stage in Greece, the predictions predictability of the cyclone formation werewas relatively poor for lead times of more than four days. It was a rather challenging issue for the ECMWF EPS to forecast precisely the intrusion of the PV streamer in the Mediterranean. This result aligns with previous studies that showed relatively poor performance in predicting medicane occurrences for lead times of the order of four to five days (Di Muzio et al., 2019). With higher confidence—, the ECMWF EPS could forecast cyclogenesis, and thus the flooding event, for shorter lead times.

During its second stage (impacts in Libya), the cyclone intensified quickly, transitioned into a medicane, makingand made landfall in Libya within a few days after its formation. The predictions operation of the medicane track and therefore its landfall-showed higher certainty for lead times for four days. These results indicate that numerical weather-prediction models are less skillful at predicting predict cyclogenesis; once, however, once the cyclone has formed, the models could become more reliable at forecasting its subsequent track. This suggests that numerical weather prediction models are more prone to an erroneous predictability of the stage of cyclogenesis, i.e., after the cyclone formed, it is more likely for a forecast model to correctly predict correctly its evolution in terms of location.

913

Precipitation amounts were found to correspond to climate extremes in both countries, Greece and Libya, where river dischargesfloods were responsible for unprecedented-floods river discharges-that largely exceeded the climatological maxima of the last 20 years. The numerical weather prediction model could forecast these climate extremes (even if thresholds were defined by reanalysis and not by the same forecast model). This underscores the exceptional potential to give the public timely, accurate warnings about the severity of impending high-impact weather events. This suggests the exceptional potential for information to the public about the severity of imminent high-impact weather. Indeed, framing weather forecasts into a climatological context, e.g., providing a precipitation event return period, would provide the means to the local population for an empirical assessment of the severity of an imminent high-impact weather event. In this context, we have analyzed Daniel concerning climate change and provided the grounds to interpret Daniel as an event whose characteristics can largely be ascribed to human-driven climate change. In these regards, we have performed an analysis based on analogues; indeed, several cyclones with similar characteristics were found during winter. The anomalous occurrence of such a storm in September, a warmer month for SST, could be a reason for enhancing its destructiveness through enhanced precipitation.

930 In the scientific literature, weather events are typically analysed as case studies with specific 931 objectives that rarely escape the narrow scope of a single scientific discipline. Here, we used Daniel, a

932 high-impact weather event, as a centrepiece of different approaches to better understand 933 socioeconomic impacts through the prism of both weather and climate scales. We find such an 934 approach valuable for linkingbridging different scientific communities and eventually 935 essentialimportant for communicating hazards to the local population. We envisage using this 936 interdisciplinary approach for other weather extremes and regions.

938 Acknowledgements

939 We gratefully acknowledge Ambrogio Volontè and an anonymous reviewer for accurately reviewing 940 our paper. This article is based upon collaborative work of two COST Actions: CA19109 941 "MedCyclones" and CA22162 "FutureMed", supported by COST – European Cooperation in Science 942 and Technology (http://www.cost.eu, last access: 14 February 2025) and from project "Earth 943 Observations as a cornerstone to the understanding and prediction of tropical like cyclone risk in the 944 Mediterranean (MEDICANES)", ESA Contract No. 4000144111/23/I-KE. Georgios Kyros from the 945 National Observatory of Athens/meteo.gr is acknowledged for helping collect the Copernicus 946 Sentinel-2 data in Figure 1. The Israel Science Foundation (grant \#978/23) funds AH's contribution. 947 PP was funded by the EU's Horizon Europe program, OCEANIDS (G.A. No. 101112919). SD 948 acknowledges the support from Next Generation EU, Mission 4, Component 1, CUP 949 B53D23007490006, project "Exploring Atmospheric Rivers in the Mediterranean and their 950 connection with extreme hydrometeorological events over Italy: observation, modelling and impacts 951 (ARMEX)".; MMM acknowledges financial support from Next Generation EU, Mission 4, 952 Component 1, CUP B53D23007360006, project "Thunderstorm outflows measurements and 953 modeling for strong WIND nowcast and RISK mitigation (WIND RISK)". We thank Franziska 954 Aemisegger for providing the msd-cpp code for the calculation of the moisture sources. 955

956 7. References

957 Argüeso, D., Marcos, M. and Amores, A.: Storm Daniel fueled by anomalously high sea surface 958 temperatures in the Mediterranean, npj Clim Atmos Sci 7, 307, 959 https://doi.org/10.1038/s41612-024-00872-2, 2024.

960

961 Avolio, E., Fanelli, C., Pisano, A. and Miglietta, M. M.: Unveiling the relationship between 962 Mediterranean tropical-like cyclones and rising Sea Surface Temperature. Geophysical Research 963 Letters 51, e2024GL109921, https://doi.org/10.1029/2024GL109921, 2024.

964

965 Beck, H. E., Van Dijk, A. I. J. M., Larraondo, P. R., McVicar, T. R., Pan, M., Dutra, E., and Miralles, 966 D. G.: MSWX: Global 3-Hourly 0.1° Bias-Corrected Meteorological Data Including Near-Real-Time 967 Updates and Forecast Ensembles, Bulletin of the American Meteorological Society, 103, E710–E732, 968 https://doi.org/10.1175/BAMS-D-21-0145.1, 2022.

969

970 Bouin, M.-N. and Lebeaupin Brossier, C.: Impact of a medicane on the oceanic surface layer from a 971 coupled, kilometre-scale simulation, Ocean Sci., 16, 1125–1142, 972 https://doi.org/10.5194/os-16-1125-2020, 2020.

973

974 Catto, J. L. and Dowdy, A.: Understanding compound hazards from a weather system perspective, 975 Weather and Climate Extremes, 32, 100313, https://doi.org/10.1016/j.wace.2021.100313, 2021. 976

976 977

977 Chaboureau, J., Pantillon, F., Lambert, D., Richard, E., and Claud, C.: Tropical transition of a 978 Mediterranean storm by jet crossing, Quart J Royal Meteoro Soc, 138, 596–611, 979 https://doi.org/10.1002/qj.960, 2012.

980

981 Couto, F. T., Kartsios, S., Lacroix, M., and Andrade, H. N.: A Quick Look at the Atmospheric 982 Circulation Leading to Extreme Weather Phenomena on a Continental Scale, Atmosphere, 15, 1205, 983 https://doi.org/10.3390/atmos15101205, 2024.

```
985 Davolio, S., Della Fera, S., Laviola, S., Miglietta, M. M., and Levizzani, V.: Heavy Precipitation over
```

- 986 Italy from the Mediterranean Storm "Vaia" in October 2018: Assessing the Role of an Atmospheric
- 987 River, Monthly Weather Review, 148, 3571–3588, https://doi.org/10.1175/MWR-D-20-0021.1, 2020.

- 989 De Vries, A. J.: A global climatological perspective on the importance of Rossby wave breaking and
- 990 intense moisture transport for extreme precipitation events, Weather Clim. Dynam., 2, 129-161,
- 991 https://doi.org/10.5194/wcd-2-129-2021, 2021.

992

- 993 Dente, E., Armon, M., and Shmilovitz, Y.: The September 2023 flood in Derna, Libya: an extreme
- 994 weather event or man-made disaster?, EGU General Assembly 2024, Vienna, Austria, 14-19 Apr
- 995 2024, EGU24-15755, https://doi.org/10.5194/egusphere-egu24-15755, 2024.

996

- 997 Di Muzio, E., Riemer, M., Fink, A. H., and Maier-Gerber, M.: Assessing the predictability of
- 998 Medicanes in ECMWF ensemble forecasts using an object-based approach, Quart J Royal Meteoro
- 999 Soc, 145, 1202–1217, https://doi.org/10.1002/qj.3489, 2019.

1000

- 1001 Dimitriou, E., Efstratiadis, A., Zotou, I., Papadopoulos, A., Iliopoulou, T., Sakki, G.-K., Mazi, K.,
- 1002 Rozos, E., Koukouvinos, A., Koussis, A. D., Mamassis, N., and Koutsoyiannis, D.: Post-Analysis of
- 1003 Daniel Extreme Flood Event in Thessaly, Central Greece: Practical Lessons and the Value of
- 1004 State-of-the-Art Water-Monitoring Networks, Water, 16, 980, https://doi.org/10.3390/w16070980,
- 1005 2024.

1006

- 1007 Faranda, D., Messori, G., and Yiou, P.: Dynamical proxies of North Atlantic predictability and
- 1008 extremes, Sci Rep, 7, 41278, https://doi.org/10.1038/srep41278, 2017.

1009

- 1010 Faranda, D., Bourdin, S., Ginesta, M., Krouma, M., Noyelle, R., Pons, F., Yiou, P., and Messori, G.: A
- 1011 climate-change attribution retrospective of some impactful weather extremes of 2021, Weather Clim.
- 1012 Dynam., 3, 1311–1340, https://doi.org/10.5194/wcd-3-1311-2022, 2022.

1013

- 1014 Faranda, D., Ginesta, M., Alberti, T., Coppola, E., and Anzidei, M.: Attributing Venice Acqua Alta
- 1015 events to a changing climate and evaluating the efficacy of MoSE adaptation strategy, npj Clim Atmos
- **1016** Sci, 6, 181, https://doi.org/10.1038/s41612-023-00513-0, 2023a.

1017

- 1018 Faranda, D., Messori, G., Coppola, E., Alberti, T., Vrac, M., Pons, F., Yiou, P., Saint Lu, M., Hisi, A.
- 1019 N. S., Brockmann, P., Dafis, S., Mengaldo, G., and Vautard, R.: ClimaMeter: contextualizing extreme
- 1020 weather in a changing climate, Weather Clim. Dynam., 5, 959–983,
- 1021 https://doi.org/10.5194/wcd-5-959-2024, 2024.

1022

- 1023 Ferrarin, C., Pantillon, F., Davolio, S., Bajo, M., Miglietta, M. M., Avolio, E., Carrió, D. S.,
- 1024 Pytharoulis, I., Sanchez, C., Patlakas, P., González-Alemán, J. J., and Flaounas, E.: Assessing the
- 1025 coastal hazard of Medicane Ianos through ensemble modelling, Nat. Hazards Earth Syst. Sci., 23,
- 1026 2273–2287, https://doi.org/10.5194/nhess-23-2273-2023, 2023a.

1027

- 1028 Ferrarin, C., Orlić, M., Bajo, M., Davolio, S., Umgiesser, G., and Lionello, P.: The contribution of a
- 1029 mesoscale cyclone and associated meteotsunami to the exceptional flood in Venice on November 12,
- 1030 2019, Quart J Royal Meteoro Soc, 149, 2929–2942, https://doi.org/10.1002/qj.4539, 2023b.

1031

- 1032 Flaounas, E., Raveh-Rubin, S., Wernli, H., Drobinski, P., and Bastin, S.: The dynamical structure of
- 1033 intense Mediterranean cyclones, Clim Dyn, 44, 2411–2427,
- 1034 https://doi.org/10.1007/s00382-014-2330-2, 2015.

- 1036 Flaounas, E., Di Luca, A., Drobinski, P., Mailler, S., Arsouze, T., Bastin, S., Beranger, K., and
- 1037 Lebeaupin Brossier, C.: Cyclone contribution to the Mediterranean Sea water budget, Clim Dyn, 46,
- 1038 913–927, https://doi.org/10.1007/s00382-015-2622-1, 2016.

```
1039
```

- 1040 Flaounas, E., Kotroni, V., Lagouvardos, K., Gray, S. L., Rysman, J.-F., and Claud, C.: Heavy rainfall
- 1041 in Mediterranean cyclones. Part I: contribution of deep convection and warm conveyor belt, Clim
- 1042 Dyn, 50, 2935–2949, https://doi.org/10.1007/s00382-017-3783-x, 2018.

- 1044 Flaounas, E., Fita, L., Lagouvardos, K., and Kotroni, V.: Heavy rainfall in Mediterranean cyclones,
- 1045 Part II: Water budget, precipitation efficiency and remote water sources, Clim Dyn, 53, 2539–2555,
- 1046 https://doi.org/10.1007/s00382-019-04639-x, 2019.

1047

- 1048 Flaounas, E., Gray, S. L., and Teubler, F.: A process-based anatomy of Mediterranean cyclones: from
- 1049 baroclinic lows to tropical-like systems, Weather Clim. Dynam., 2, 255–279,
- 1050 https://doi.org/10.5194/wcd-2-255-2021, 2021.

1051

- 1052 Flaounas, E., Davolio, S., Raveh-Rubin, S., Pantillon, F., Miglietta, M. M., Gaertner, M. A., Hatzaki,
- 1053 M., Homar, V., Khodayar, S., Korres, G., Kotroni, V., Kushta, J., Reale, M., and Ricard, D.:
- 1054 Mediterranean cyclones: current knowledge and open questions on dynamics, prediction, climatology
- **1055** and impacts, Weather Clim. Dynam., 3, 173–208, https://doi.org/10.5194/wcd-3-173-2022, 2022.

1056

- 1057 Flaounas, E., Aragão, L., Bernini, L., Dafis, S., Doiteau, B., Flocas, H., Gray, S. L., Karwat, A.,
- 1058 Kouroutzoglou, J., Lionello, P., Miglietta, M. M., Pantillon, F., Pasquero, C., Patlakas, P., Picornell,
- 1059 M. Á., Porcù, F., Priestley, M. D. K., Reale, M., Roberts, M. J., Saaroni, H., Sandler, D., Scoccimarro,
- 1060 E., Sprenger, M., and Ziv, B.: A composite approach to produce reference datasets for extratropical
- 1061 cyclone tracks: application to Mediterranean cyclones, Weather Clim. Dynam., 4, 639–661,
- 1062 https://doi.org/10.5194/wcd-4-639-2023, 2023.

1063

- 1064 Grimaldi, S., Salamon, P., Disperati, J., Zsoter, E., Russo, C., Ramos, A., Carton De Wiart, C.,
- 1065 Barnard, C., Hansford, E., Gomes, G., Prudhomme, C. (2022): River discharge and related historical
- 1066 data from the Global Flood Awareness System. v4.0. European Commission, Joint Research Centre
- 1067 (JRC). URL: https://cds.climate.copernicus.eu/cdsapp#!/dataset/cems-glofas-historical (Accessed on
- 1068 09-Oct-2023)

1069

- 1070 Global Data Institute of the UN International Organization for Migration (IOM). 2023. Libya —
- 1071 Storm Daniel Flash update 83 (134 October September 2023)

1072

- 1073 He, K., Yang, Q., Shen, X., Dimitriou, E., Mentzafou, A., Papadaki, C., Stoumboudi, M., and
- 1074 Anagnostou, E. N.: Brief communication: Storm Daniel Flood Impact in Greece 2023: Mapping Crop
- 1075 and Livestock Exposure from SAR, https://doi.org/10.5194/nhess-2023-173, 12 October 2023.

1076

- 1077 Hersbach, H., Bell, B., Berrisford, P., Hirahara, S., Horányi, A., Muñoz-Sabater, J., Nicolas, J.,
- 1078 Peubey, C., Radu, R., Schepers, D., Simmons, A., Soci, C., Abdalla, S., Abellan, X., Balsamo, G.,
- 1079 Bechtold, P., Biavati, G., Bidlot, J., Bonavita, M., De Chiara, G., Dahlgren, P., Dee, D., Diamantakis,
- 1080 M., Dragani, R., Flemming, J., Forbes, R., Fuentes, M., Geer, A., Haimberger, L., Healy, S., Hogan,
- 1081 R. J., Hólm, E., Janisková, M., Keeley, S., Laloyaux, P., Lopez, P., Lupu, C., Radnoti, G., De Rosnay,
- 1082 P., Rozum, I., Vamborg, F., Villaume, S., and Thépaut, J.: The ERA5 global reanalysis, Quart J Royal
- 1083 Meteoro Soc, 146, 1999–2049, https://doi.org/10.1002/qj.3803, 2020.

1084

- 1085 Hewson, T., Ashoor, A., Boussetta, S., Emanuel, K., Lagouvardos, K., Lavers, D., Magnusson, L.,
- 1086 Pillosu, F., Zsoter, E., Medicane Daniel: an extraordinary cyclone with devastating impacts, ECMWF
- 1087 newsletters 179, 2024, 33-47.

1088

- 1089 Hochman, A., Scher, S., Quinting, J., Pinto, J. G., and Messori, G.: Dynamics and predictability of
- 1090 cold spells over the Eastern Mediterranean, Clim Dyn, 58, 2047–2064,
- 1091 https://doi.org/10.1007/s00382-020-05465-2, 2022a.

1092

1093 Hochman, A., Marra, F., Messori, G., Pinto, J. G., Raveh-Rubin, S., Yosef, Y., and Zittis, G.: Extreme

```
1094 weather and societal impacts in the eastern Mediterranean, Earth Syst. Dynam., 13, 749–777,
```

1095 https://doi.org/10.5194/esd-13-749-2022, 2022b.

1096

- 1097 Hochman, A., Plotnik, T., Marra, F., Shehter, E.-R., Raveh-Rubin, S., and Magaritz-Ronen, L.: The
- 1098 sources of extreme precipitation predictability; the case of the 'Wet' Red Sea Trough, Weather and
- 1099 Climate Extremes, 40, 100564, https://doi.org/10.1016/j.wace.2023.100564, 2023.

1100

- 1101 Hochman, A., Shachar, N., and Gildor, H.: Unraveling sub-seasonal precipitation variability in the
- 1102 Middle East via Indian Ocean sea surface temperature, Sci Rep, 14, 2919,
- 1103 https://doi.org/10.1038/s41598-024-53677-x, 2024.

1104

- 1105 Hodgkins, G. A., Whitfield, P. H., Burn, D. H., Hannaford, J., Renard, B., Stahl, K., ... & Wilson, D.
- 1106 (2017). Climate-driven variability in the occurrence of major floods across North America and
- **1107** Europe. Journal of Hydrology, 552, 704-717.

1108

- 1109 IFRC (International Federation of Red Cross and Red Crescent Societies). World Disasters Report
- 1110 2020 Executive Summary. https://www.ifrc.org/document/world-disasters-report-2020

1111

- 1112 Khodayar, S., Davolio, S., Di Girolamo, P., Lebeaupin Brossier, C., Flaounas, E., Fourrie, N., Lee,
- 1113 K.-O., Ricard, D., Vie, B., Bouttier, F., Caldas-Alvarez, A., and Ducrocq, V.: Overview towards
- 1114 improved understanding of the mechanisms leading to heavy precipitation in the western
- 1115 Mediterranean: lessons learned from HyMeX, Atmos. Chem. Phys., 21, 17051–17078,
- 1116 https://doi.org/10.5194/acp-21-17051-2021, 2021.

1117

- 1118 Khodayar, S., Kushta, J., Catto, J. L., Dafis, S., Davolio, S., Ferrarin, C., Flaounas, E., Groenemeijer,
- 1119 P., Hatzaki, M., Hochman, A., Kotroni, V., Landa, J., Láng-Ritter, I., Lazoglou, G., Liberato, M. L. R.,
- 1120 Miglietta, M. M., Papagiannaki, K., Patlakas, P., Stojanov, R., and Zittis, G.: Mediterranean Cyclones
- 1121 in a Changing Climate: A Review on Their Socio-Economic Impacts, Reviews of Geophysics, 63,
- 1122 e2024RG000853, https://doi.org/10.1029/2024RG000853, 2025.

1123

- 1124 Korres, G., Ravdas, M., Denaxa, D., & Sotiropoulou, M. (2021). Mediterranean Sea Waves
- 1125 Reanalysis INTERIM (CMEMS Med-Waves, MedWAM3I system) (Version 1) [Data set]. Copernicus
- 1126 Monitoring Environment Marine Service (CMEMS).
- 1127 https://doi.org/10.25423/CMCC/MEDSEA\_MULTIYEAR\_WAV\_006\_012\_MEDWAM3I

1128

- 1129 Korres, G., Oikonomou, C., Denaxa, D., & Sotiropoulou, M. (2023). Mediterranean Sea Waves
- 1130 Analysis and Forecast (Copernicus Marine Service MED-Waves, MEDWAM4 system) (Version 1)
- 1131 [Data set]. Copernicus Marine Service (CMS).
- 1132 https://doi.org/10.25423/CMCC/MEDSEA\_ANALYSISFORECAST\_WAV\_006\_017\_MEDWAM4

1133

- 1134 Lagouvardos, K., Kotroni, V., Bezes, A., Koletsis, I., Kopania, T., Lykoudis, S., Mazarakis, N.,
- 1135 Papagiannaki, K., and Vougioukas, S.: The automatic weather stations NOANN network of the
- 1136 National Observatory of Athens: operation and database, Geoscience Data Journal, 4, 4–16,
- 1137 https://doi.org/10.1002/gdj3.44, 2017.
- 1138 Maslova, V., Voskresenskaya, E. N., & Lubkov, A. (2017). Multidecadal change of winter cyclonic
- 1139 activity in the Mediterranean associated with AMO and PDO. Terrestrial, Atmospheric and Oceanic
- 1140 Sciences, 28(6), 965–977. https://doi.org/10.3319/TAO.2017.04.23.01

1141

- 1142 Messmer, M., Gómez-Navarro, J. J., and Raible, C. C.: Sensitivity experiments on the response of Vb
- 1143 cyclones to sea surface temperature and soil moisture changes, Earth Syst. Dynam., 8, 477–493,
- 1144 https://doi.org/10.5194/esd-8-477-2017, 2017.

1145

1146 Miglietta, M. M., Moscatello, A., Conte, D., Mannarini, G., Lacorata, G., and Rotunno, R.: Numerical

```
1147 analysis of a Mediterranean 'hurricane' over south-eastern Italy: Sensitivity experiments to sea
```

- 1148 surface temperature, Atmospheric Research, 101, 412–426,
- 1149 https://doi.org/10.1016/j.atmosres.2011.04.006, 2011.
- 1150
- 1151 Miglietta, M. M., Carnevale, D., Levizzani, V., and Rotunno, R.: Role of moist and dry air advection
- 1152 in the development of Mediterranean tropical-like cyclones (medicanes), Quart J Royal Meteoro Soc,
- 1153 147, 876–899, https://doi.org/10.1002/qj.3951, 2021.
- 1154
- 1155 Miglietta M. M., González-Alemán J. J., Panegrossi G., Gaertner M. A., Pantillon F., Pasquero C.,
- 1156 Schultz D. M., D'Adderio L. P., Dafis S., Husson R., Ricchi A., Carrió D. S., Davolio S., Fita L.,
- 1157 Picornell M. A., Pytharoulis I., Raveh-Rubin S., Scoccimarro E., Bernini L., Cavicchia L., Conte D.,
- 1158 Ferretti R., Flocas H., Gutiérrez-Fernández J., Hatzaki M., Homar Santaner V., Jansà A., Patlakas P.,
- 1159 Flaounas E., Defining Medicanes: Bridging the Knowledge Gap Between Tropical and Extratropical
- 1160 Cyclones in the Mediterranean, Bull. Am. Meteor. Soc., submitted
- 1161
- 1162 Nissen, K. M., Leckebusch, G. C., Pinto, J. G., Renggli, D., Ulbrich, S., and Ulbrich, U.: Cyclones
- 1163 causing wind storms in the Mediterranean: characteristics, trends and links to large-scale patterns,
- 1164 Nat. Hazards Earth Syst. Sci., 10, 1379–1391, https://doi.org/10.5194/nhess-10-1379-2010, 2010.
- 1165
- 1166 Pantillon, F. P., Chaboureau, J.-P., Mascart, P. J., and Lac, C.: Predictability of a Mediterranean
- 1167 Tropical-Like Storm Downstream of the Extratropical Transition of Hurricane Helene (2006),
- 1168 Monthly Weather Review, 141, 1943–1962, https://doi.org/10.1175/MWR-D-12-00164.1, 2013.
- 1169
- 1170 Pantillon, F., Davolio, S., Avolio, E., Calvo-Sancho, C., Carrió, D. S., Dafis, S., Gentile, E. S.,
- 1171 Gonzalez-Aleman, J. J., Gray, S., Miglietta, M. M., Patlakas, P., Pytharoulis, I., Ricard, D., Ricchi, A.,
- 1172 Sanchez, C., and Flaounas, E.: The crucial representation of deep convection for the cyclogenesis of
- **1173** Medicane Ianos, Weather Clim. Dynam., 5, 1187–1205, https://doi.org/10.5194/wcd-5-1187-2024, **1174** 2024.
- 1175
- 1176 Patlakas, P., Stathopoulos, C., Tsalis, C., and Kallos, G.: Wind and wave extremes associated with
- 1177 tropical-like cyclones in the Mediterranean basin, Intl Journal of Climatology, 41
- 1178 https://doi.org/10.1002/joc.6795, 2021.
- 1179
- 1180 Pfahl, S. and Wernli, H.: Quantifying the Relevance of Cyclones for Precipitation Extremes, Journal
- 1181 of Climate, 25, 6770–6780, https://doi.org/10.1175/JCLI-D-11-00705.1, 2012.
- 1182
- 1183 Portal, A., Raveh-Rubin, S., Catto, J. L., Givon, Y., and Martius, O.: Linking compound weather
- 1184 extremes to Mediterranean cyclones, fronts, and airstreams, Weather Clim. Dynam., 5, 1043–1060,
- 1185 https://doi.org/10.5194/wcd-5-1043-2024, 2024.
- 1186
- 1187 Pytharoulis, I.: Analysis of a Mediterranean tropical-like cyclone and its sensitivity to the sea surface
- 1188 temperatures, Atmospheric Research, 208, 167–179, https://doi.org/10.1016/j.atmosres.2017.08.009,
- **1189** 2018.
- 1190
- 1191 Qiu J., Zhao W., Brocca L., Paolo Tarolli (2023). Storm Daniel revealed the fragility of the
- 1192 Mediterranean region. The Innovation Geoscience 1(3), 100036.
- 1193 https://doi.org/10.59717/j.xinn-geo.2023.100036
- 1194
- 1195 Raveh-Rubin, S. and Flaounas, E.: A dynamical link between deep Atlantic extratropical cyclones and
- 1196 intense Mediterranean cyclones, Atmospheric Science Letters, 18, 215–221,
- 1197 https://doi.org/10.1002/asl.745, 2017.
- 1198
- 1199 Raveh-Rubin, S. and Wernli, H.: Large-scale wind and precipitation extremes in the Mediterranean:
- 1200 dynamical aspects of five selected cyclone events, Quart J Royal Meteoro Soc, 142, 3097-3114,
- 1201 https://doi.org/10.1002/qj.2891, 2016.

```
1202
```

- 1203 Reale, M., Cabos Narvaez, W. D., Cavicchia, L., Conte, D., Coppola, E., Flaounas, E., Giorgi, F.,
- 1204 Gualdi, S., Hochman, A., Li, L., Lionello, P., Podrascanin, Z., Salon, S., Sanchez-Gomez, E.,
- 1205 Scoccimarro, E., Sein, D. V., and Somot, S.: Future projections of Mediterranean cyclone
- 1206 characteristics using the Med-CORDEX ensemble of coupled regional climate system models, Clim
- 1207 Dyn, 58, 2501–2524, https://doi.org/10.1007/s00382-021-06018-x, 2022.

- 1209 Ricchi, A., Miglietta, M. M., Barbariol, F., Benetazzo, A., Bergamasco, A., Bonaldo, D., Cassardo, C.,
- 1210 Falcieri, F. M., Modugno, G., Russo, A., Sclavo, M., and Carniel, S.: Sensitivity of a Mediterranean
- 1211 tropical-like cyclone to different model configurations and coupling strategies, Atmosphere, 8, 1–32,
- 1212 https://doi.org/10.3390/atmos8050092, 2017.

1213

- 1214 Romaniello, V., Oddo, P., Tonani, M., Torrisi, L., Grandi, A., and Pinardi, N.: Impact of Sea Surface
- 1215 Temperature on COSMO Forecasts of a Medicane over the Western Mediterranean Sea, JEASE, 5,
- 1216 https://doi.org/10.17265/2159-581X/2015.06.002, 2015.

1217

- 1218 Romero, R. and Emanuel, K.: Climate Change and Hurricane-Like Extratropical Cyclones:
- 1219 Projections for North Atlantic Polar Lows and Medicanes Based on CMIP5 Models, J. Climate, 30,
- 1220 279–299, https://doi.org/10.1175/JCLI-D-16-0255.1, 2017.

1221

- 1222 Rousseau-Rizzi, R., Raveh-Rubin, S., Catto, J. L., Portal, A., Givon, Y., and Martius, O.: A
- 1223 storm-relative climatology of compound hazards in Mediterranean cyclones, Weather Clim. Dynam.,
- 1224 5, 1079–1101, https://doi.org/10.5194/wcd-5-1079-2024, 2024.

1225

- 1226 Sanchez, C., Gray, S., Volonte', A., Pantillon, F., Berthou, S., and Davolio, S.: The impact of
- 1227 preceding convection on the development of Medicane Ianos and the sensitivity to sea surface
- 1228 temperature. Weather Clim. Dynam., 5, 1429 1455, https://doi.org/10.5194/wcd-5-1429-2024, 2024.

1229

- 1230 Sandler, D., Saaroni, H., Ziv, B., Hochman, A., Harnik, N., and Rostkier-Edelstein, D.: A multiscale
- 1231 approach to statistical downscaling of daily precipitation: Israel as a test case, Intl Journal of
- **1232** Climatology, 44, 59–71, https://doi.org/10.1002/joc.8315, 2024.

1233

- 1234 Scherrmann, A., Wernli, H., and Flaounas, E.: The upstream-downstream connection of North
- 1235 Atlantic and Mediterranean cyclones in semi-idealized simulations, Weather Clim. Dynam., 5,
- 1236 419-438, https://doi.org/10.5194/wcd-5-419-2024, 2024.

1237

- 1238 Shirzaei, M., Vahedifard, F., Sadhasivam, N., Ohenhen, L., Dasho, O., Tiwari, A., Werth, S., Azhar,
- 1239 M., Zhao, Y., Nicholls, R. J., and AghaKouchak, A.: Aging dams, political instability, poor human
- 1240 decisions and climate change: recipe for human disaster, npj Nat. Hazards, 2, 1–8,
- 1241 https://doi.org/10.1038/s44304-024-00056-1, 2025.

1242

- 1243 Sioni, F., Davolio, S., Grazzini, F., and Giovannini, L.: Revisiting the atmospheric dynamics of the
- 1244 two century floods over north-eastern Italy. Atmos. Research, 286, 106662,
- 1245 https://doi.org/10.1016/j.atmosres.2023.106662, 2023.

1246

- 1247 Sodemann, H., Schwierz, C., and Wernli, H.: Interannual variability of Greenland winter precipitation
- 1248 sources: Lagrangian moisture diagnostic and North Atlantic Oscillation influence, J. Geophys. Res.,
- 1249 113, 2007JD008503, https://doi.org/10.1029/2007JD008503, 2008.

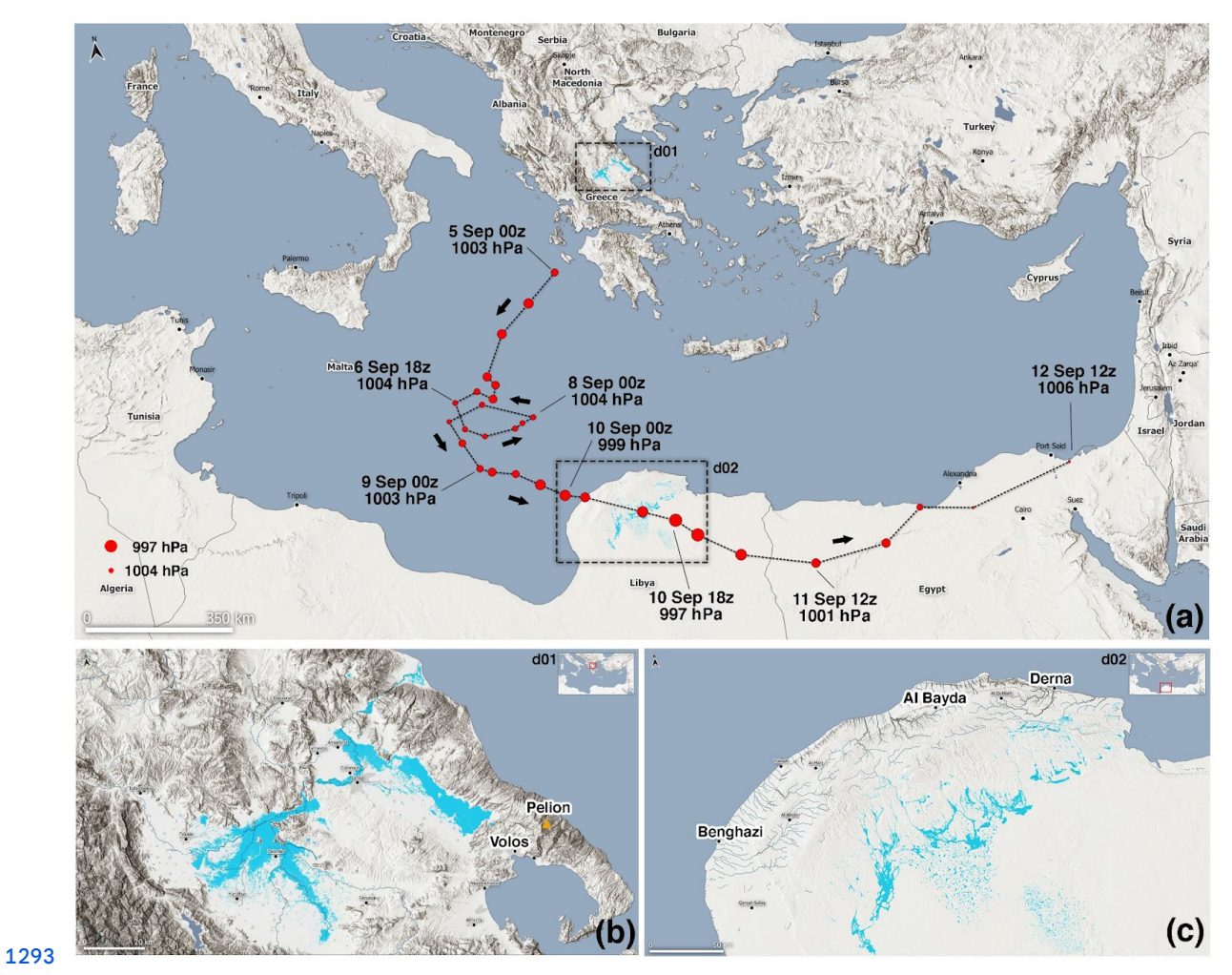
1250

- 1251 Sprenger, M. and Wernli, H.: The LAGRANTO Lagrangian analysis tool version 2.0, Geosci. Model
- **1252** Dev., 8, 2569–2586, https://doi.org/10.5194/gmd-8-2569-2015, 2015.

1253

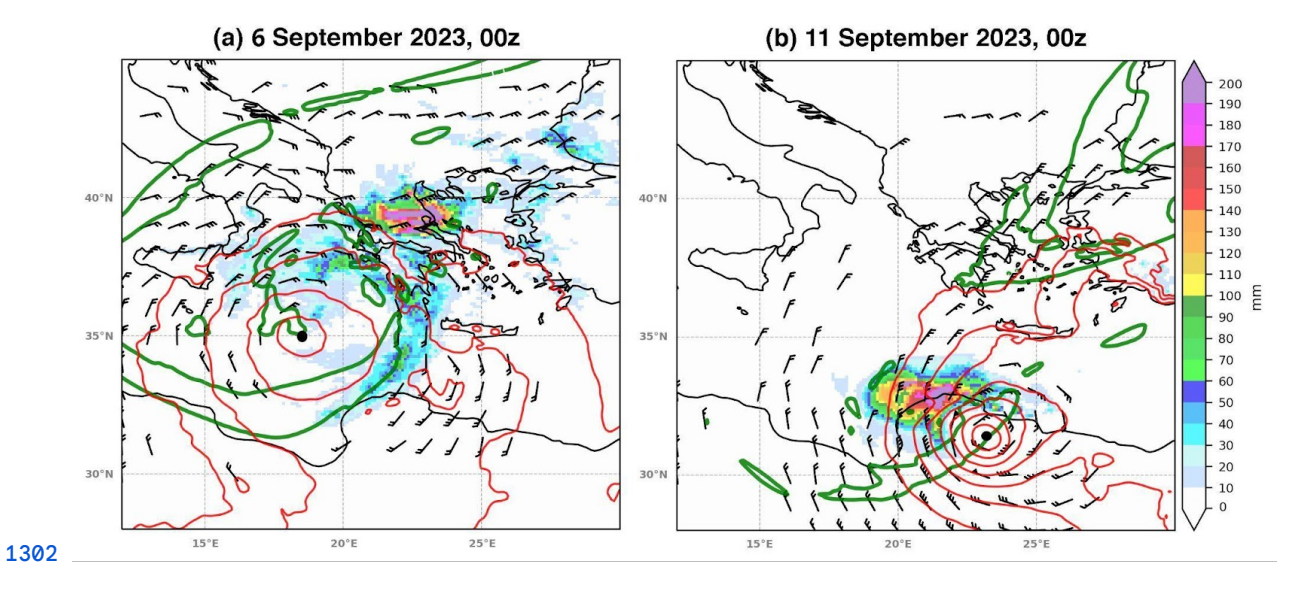
1254 UNICEF. 2023. Libya Storm Daniel & Flooding, Situation Report #1. (14-09-2023)

```
1255
1256 United Nations Office for the Coordination of Humanitarian Affairs (OCHA). 2023. Flash Appeal
1257 Libya.
1258
1259 Varlas, G., Vervatis, V., Spyrou, C., Papadopoulou, E., Papadopoulos, A., and Katsafados, P.:
1260 Investigating the impact of atmosphere—wave—ocean interactions on a Mediterranean tropical-like
1261 cyclone, Ocean Model., 153, 101675, https://doi.org/10.1016/j.ocemod.2020.101675, 2020.
1262 ¶
1263 Romaniello, V., Oddo, P., Tonani, M., Torrisi, L., Grandi, A., and Pinardi, N.: Impact of Sea Surface-
1264 Temperature on GOSMO Forecasts of a Medicane over the Western Mediterranean Sea, JEASE, 5,
1265 https://doi.org/10.17265/2159-581X/2015.06.002, 2015.
1266
1267 World Weather
                                              Meteorological
                                                                                         Organisation:
1268 https://wmo.int/media/news/libya-floods-show-need-multi-hazard-early-warnings-unified-response,
1269 2023a, last access: 10 March 2024.
1270
1271 World Weather
                                              Meteorological
                                                                                         Organisation:
1272 https://wmo.int/media/news/storm-daniel-leads-extreme-rain-and-floods-mediterranean-heavy-loss-of-
1273 life-libya, 2023b, last access: 3 February, 2025
1274
1275 Wernli, H. and Davies, H. C.: A Lagrangian-based analysis of extratropical cyclones. I: The method
1276 and
             some
                      applications,
                                      Quart
                                                      Royal
                                                                Meteoro
                                                                            Soc,
                                                                                    123,
                                                                                             467-489,
                                                J
1277 https://doi.org/10.1002/qj.49712353811, 1997.
1278
1279 World Bank, 2023. Libya Storm and Flooding 2023. Rapid Damage and Needs Assessment.
1280 Washington, DC: World Bank, http://recovery.preventionweb.net/quick/82808.
1281
1282
1283
1284
1285
1286
1287
1288
1289
1290
1291
1292 Figures
```

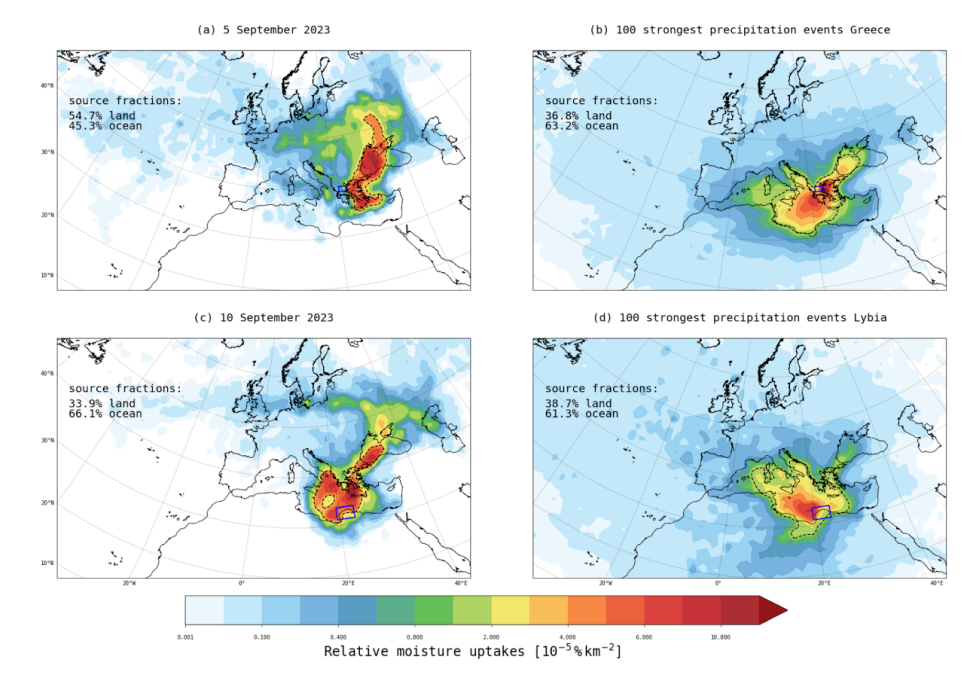


**1294 Figure 1 (a)** Track of Storm Daniel at six-hour intervals based on ECMWF analysis, where the size of 1295 red dots is proportional to cyclone depth in terms of minimum MSLPmean sea level pressure. Flooded 1296 areas are shown in cyan and blue tones (acquired by one of the Copernicus Sentinel-2 satellites on 10 1297 and 12 September 2023). Panels **(b)** and **(c)** zoom over central Greece and Libya (square boxes d01 1298 and d02 in panel a).

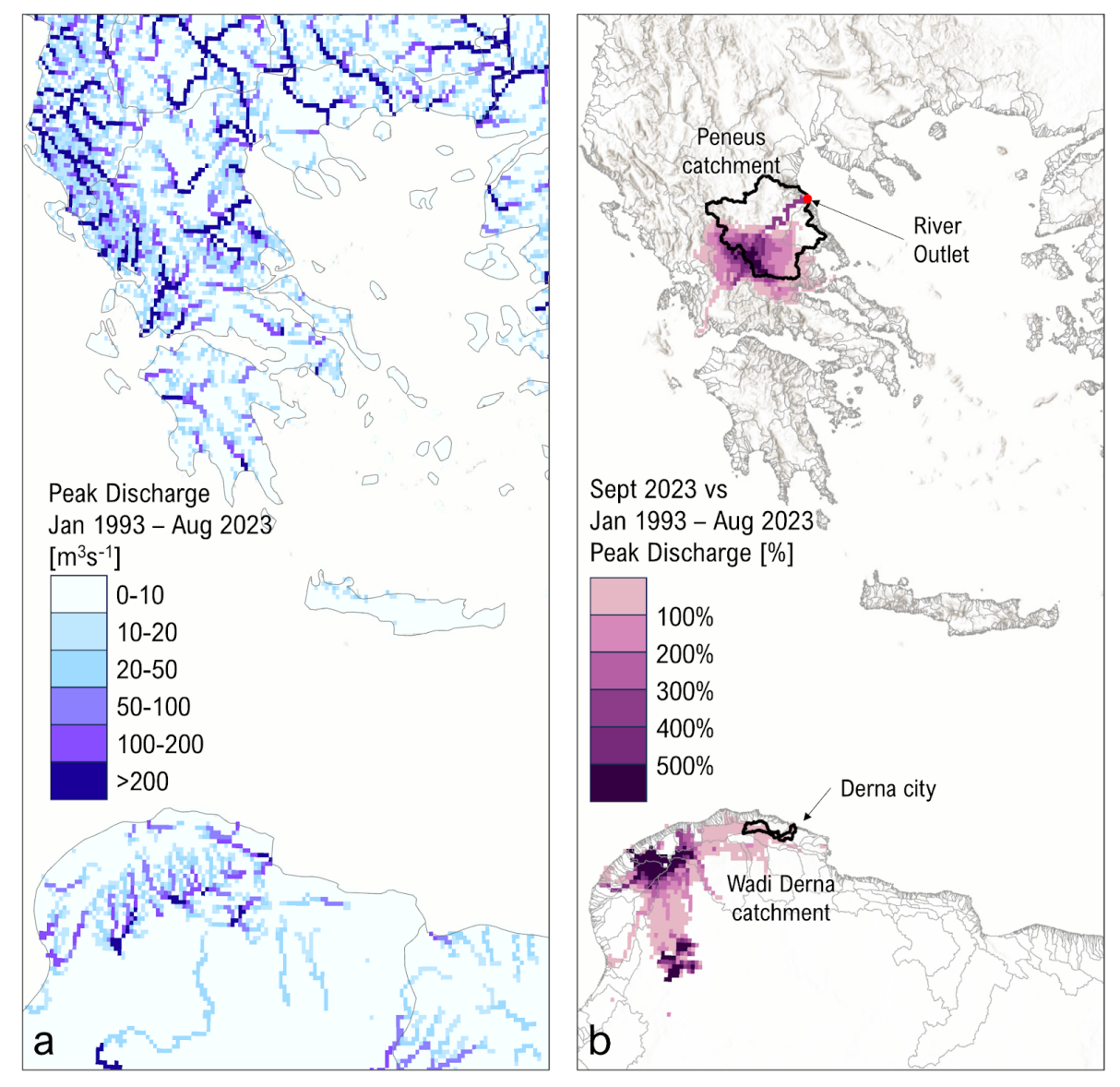




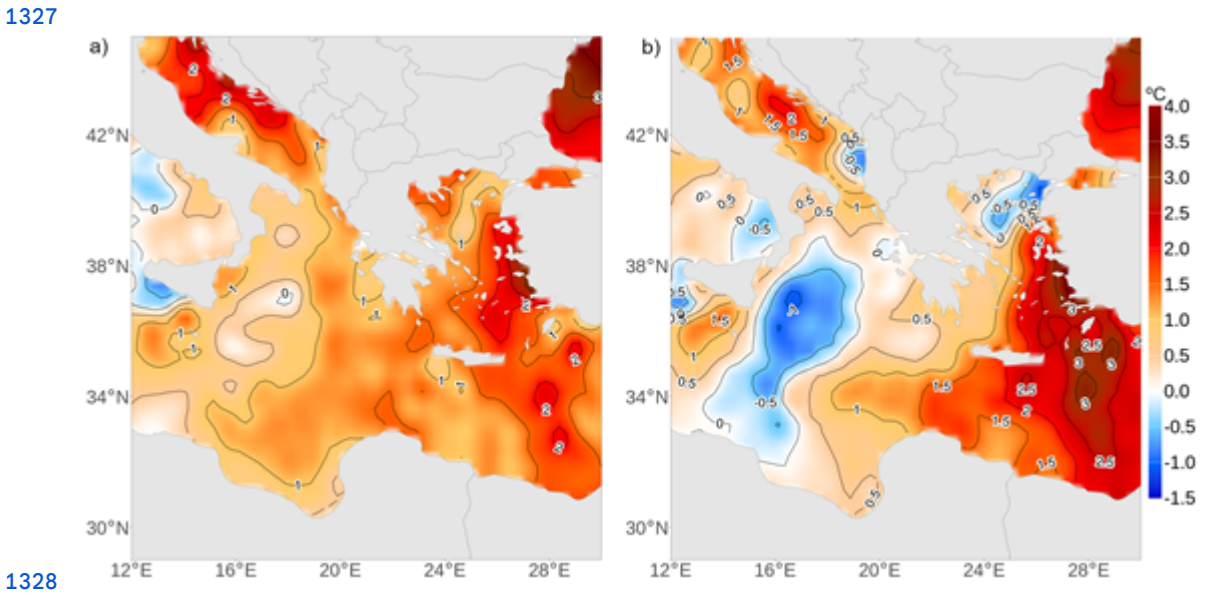
**1303 Figure 2 (a)** Potential Vorticity of 2 PVU at 300 hPa (in green contour) and wind speed higher than 15 1304 knots at 850 hPa (in barbs, with full and half bars depicting 10 and 5 knots, respectively) and 1305 MSLPmean sea level pressure (in red contours for values lower than 1012 hPa with 2 hPa interval) on 1306 6 September 2023, at 00 UTC. 24-hour total accumulated precipitation from 5 to 6 of September 00 1307 UTC is shown in shading (max value 434 mm). **(b)** Same as **(a)** but for 11 September 2023, at 00 1308 UTC (max precipitation value 382 mm). The black dot indicates the minimum MSLPmean sea level 1309 pressure position in both panels.



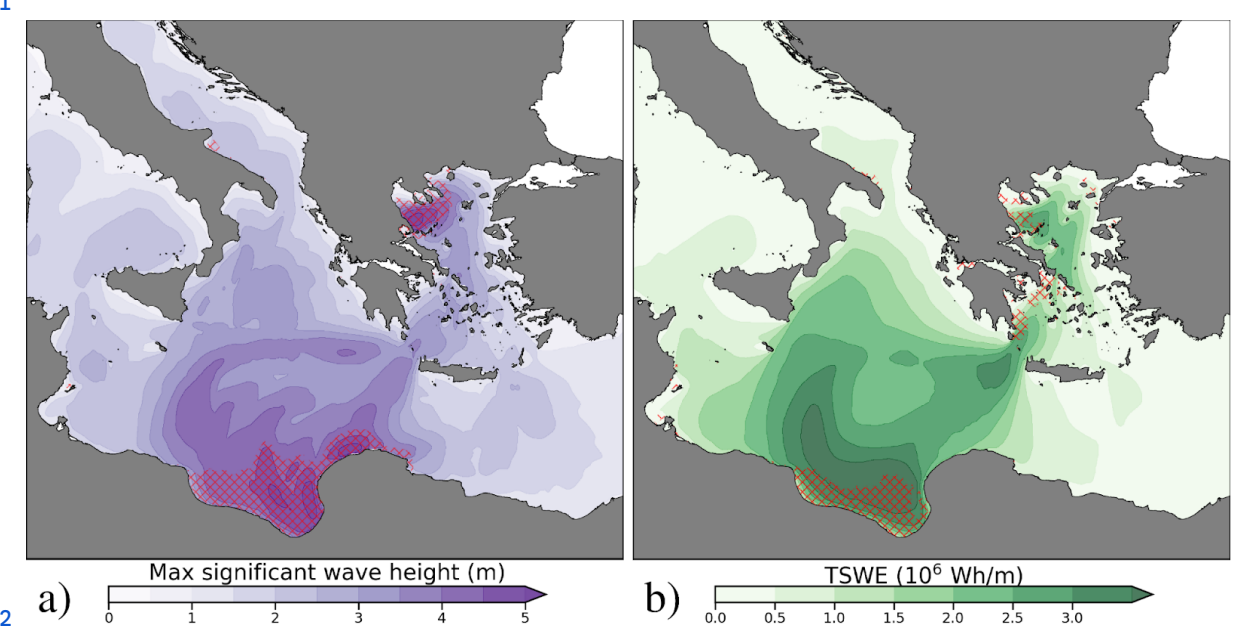
**1312 Figure 3 (a) Relative** moisture uptakes that contribute to the precipitation event in Thessaly (depicted **1313** with the blue rectangle) on 5 September 2023. The black dashed contour outlines the largest moisture **1314** source regions, which account for 50% of the total moisture uptake. The numbers on the top left show **1315** the relative land and ocean fraction of the moisture sources. **(b)** as in **(a)** but for the 100 most extreme **1316** daily precipitation events in Thessaly from 1990 to 2023. **(c)** as in **(a)** but for the precipitation in the **1317** study region in Libya (blue rectangle) on 10 September 2023. **(d)** as in **(b)** but for Libya.



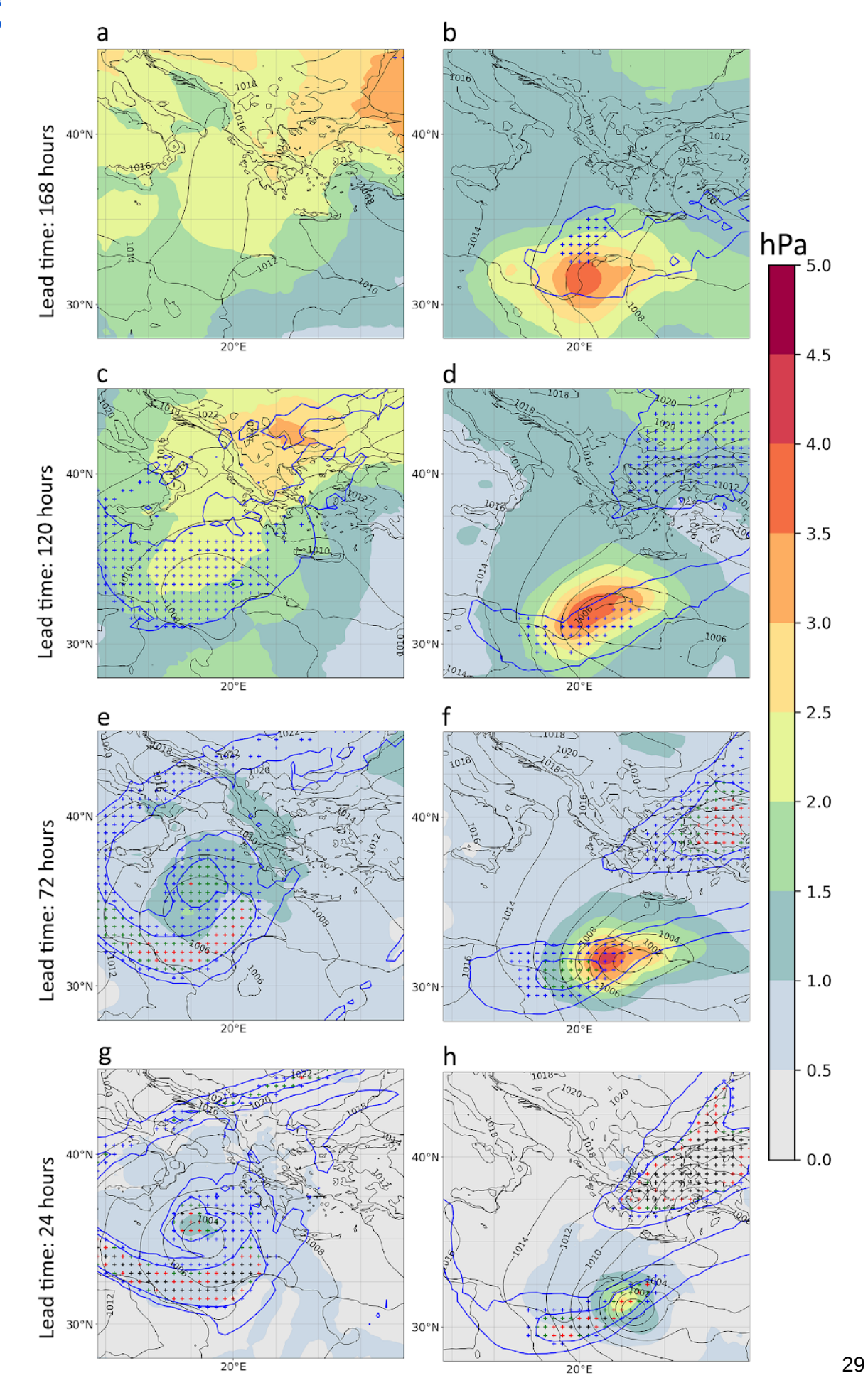
**1320 Figure 4** Peak discharge over three recent decades (Jan 1993 – Aug 2023) versus Daniel storm as **1321** represented by the Global Flood Awareness System (**a**) spatial distribution of the maximum peak river **1322** discharge from January 1993 to August 2023, (**b**) comparison map for September 2023 illustrating the **1323** event-wide peak river discharges as a percentage increase over the maximum peak river discharges **1324** during the 30 years January in (**a**).



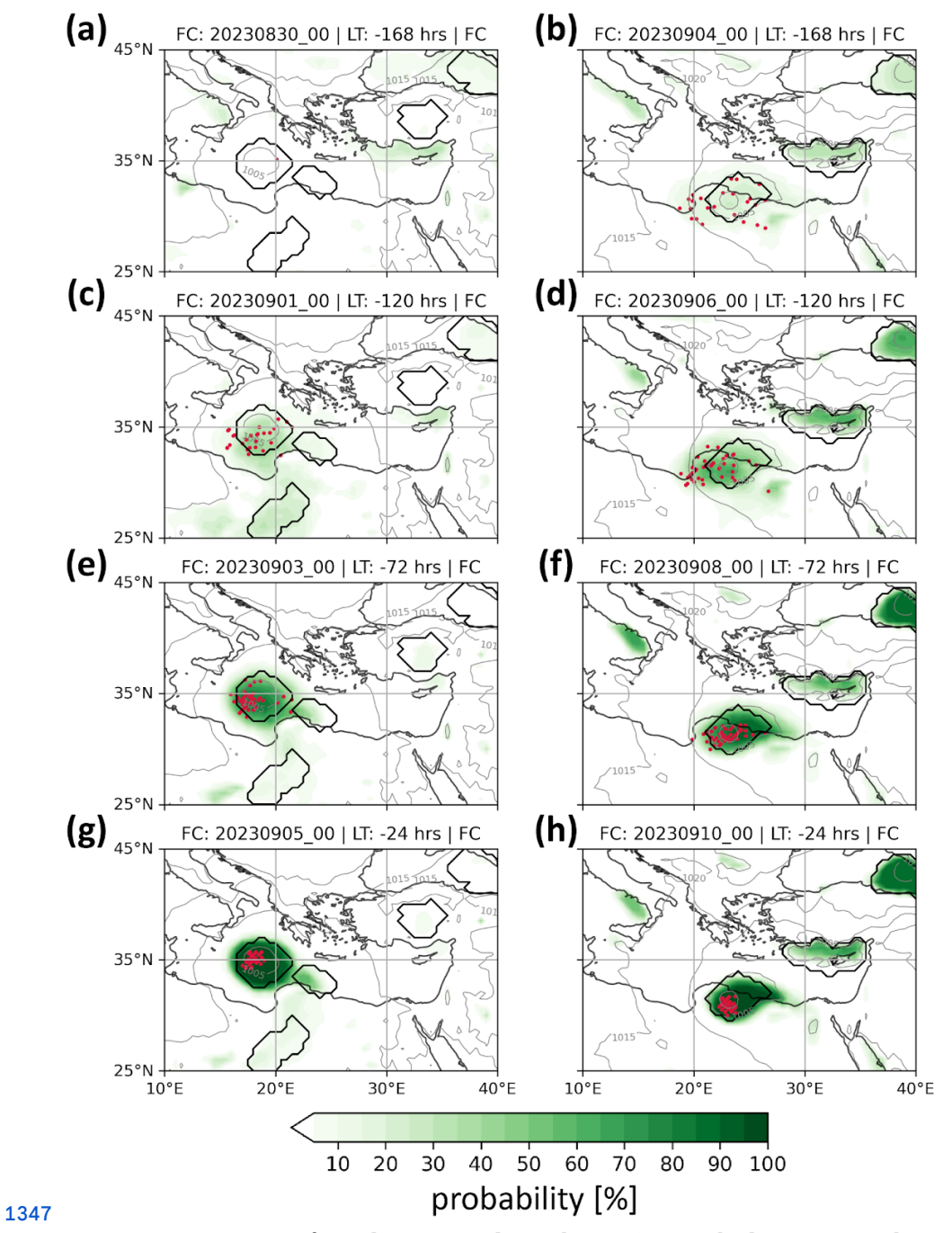
**1329 Figure 5 (a)** Daily SST anomaly from ERA5, for 3 September 2023, and (b) 9 September 2023. The **1330** reference climatology for anomaly determination is 1982-2011.



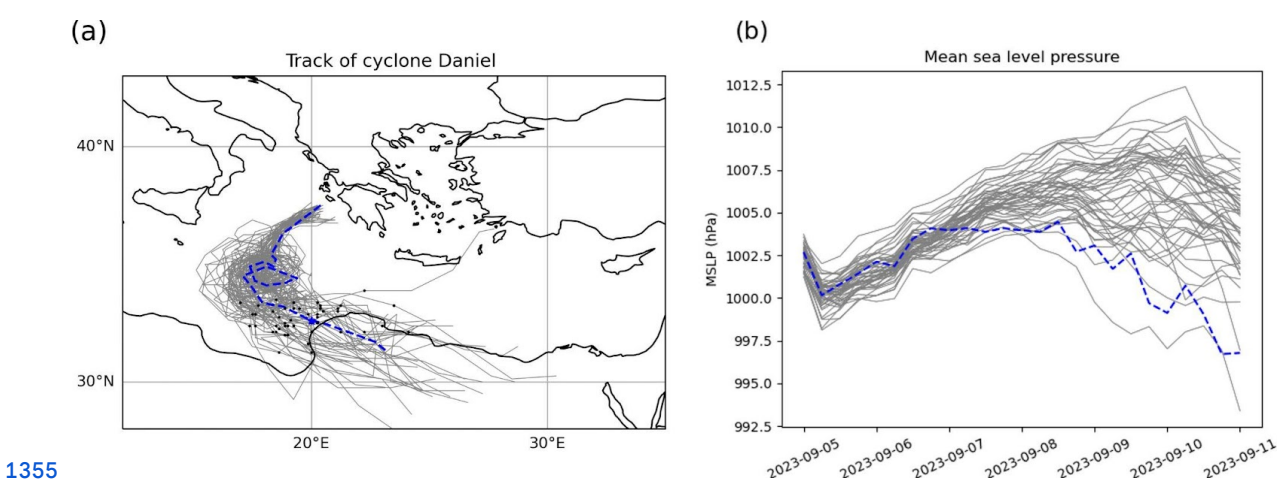
**Figure 6 (a)** Maximum significant wave height. **(b)** Total wave energy of the storm. Purple (a) and 1334 red (b) patches mark areas of extreme conditions (above the 99th percentile) determined based on the 1335 Mediterranean Sea wave reanalysis.



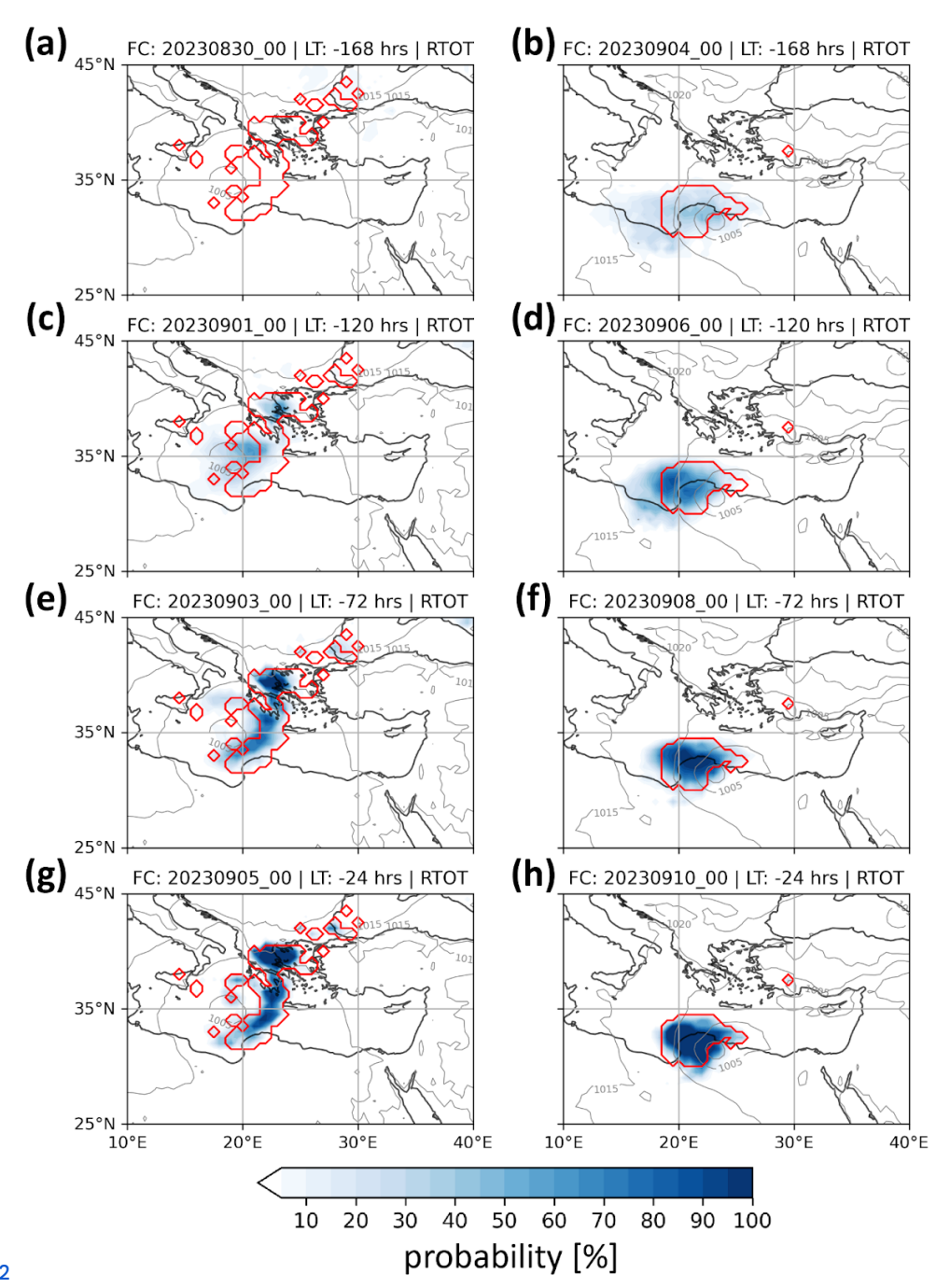
**Figure 7** Standard deviation (in colour shading) and average (in black contour) MSLP from the 51 1341 ensemble members of the ECMWF EPS. Blue contours enclose areas with a median equal to 1 and 2 1342 PVU at 300 hPa among all members of the EPS. Blue crosses indicate areas where at least 25% of the 1343 members have PV values greater than 2 PVU. Green, red, and black crosses denote agreement by at 1344 least 50%, 75%, and 95% of the members, respectively. Panels depict different lead forecast times 1345 valid on 6 September at 00 UTC (panels **a**, **c**, **e**, **g**) and 11 September at 00 UTC (**b**, **d**, **f**, **h**). 1346



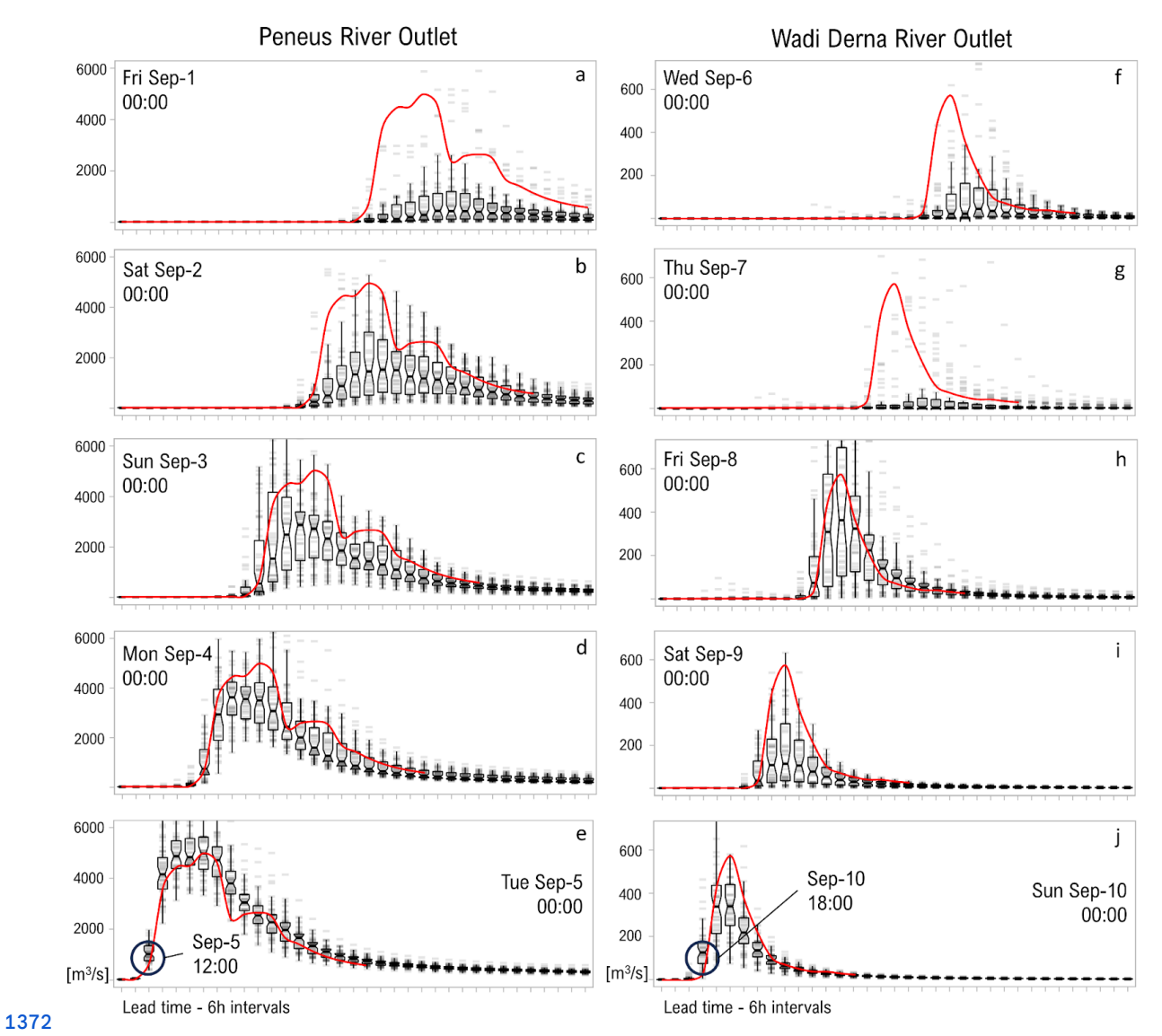
**Figure 8** Percentage of overlapping cyclone objects (green shading) among the ensemble prediction 1349 system members for different lead times valid on 6 September 2023, 00 UTC (left column panels) 1350 and 11 September 2023, 00 UTC (right column panels). Black contours show cyclone objects in 1351 ECMWF analysis (grey contours for MSLP isobars in ECMWF analysis). Red dots depict the location 1352 of the minimum MSLPpressure of Daniel in the ensemble members.



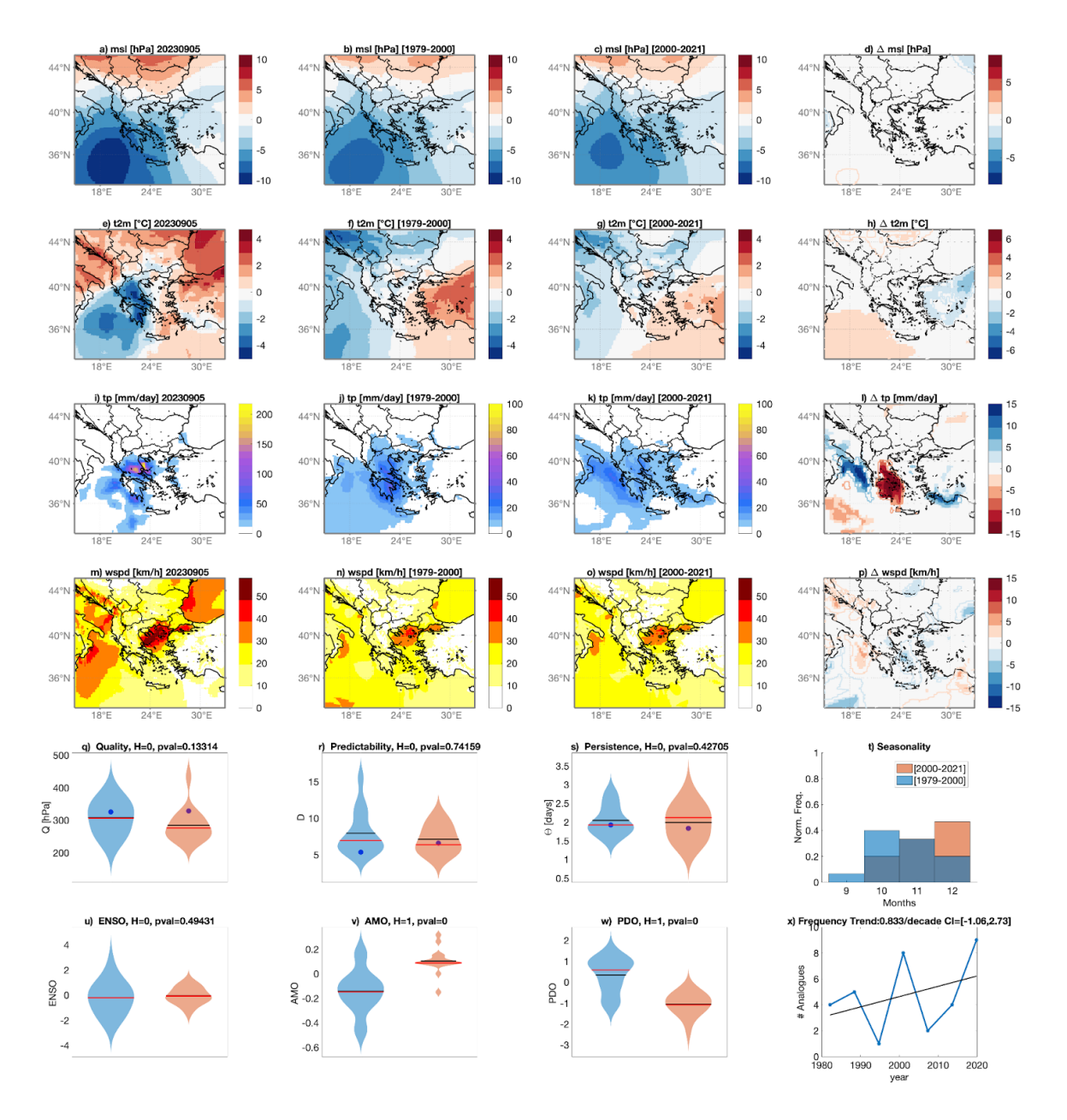
**1356 Figure 9 (a)** Cyclone tracks based on MSLP at the centre of cyclone Daniel as represented by the **1357** ECMWF analysis (blue dashed line) and by the 50 members of the EPS of ECMWF (grey lines), **1358** initialized on 5 September at 00 UTC. Black dots in (a) depict the cyclone location on 10 September, **1359** 00 UTC (**b)** As in (**a)** but as time series of minimum MSLP. **1360** 



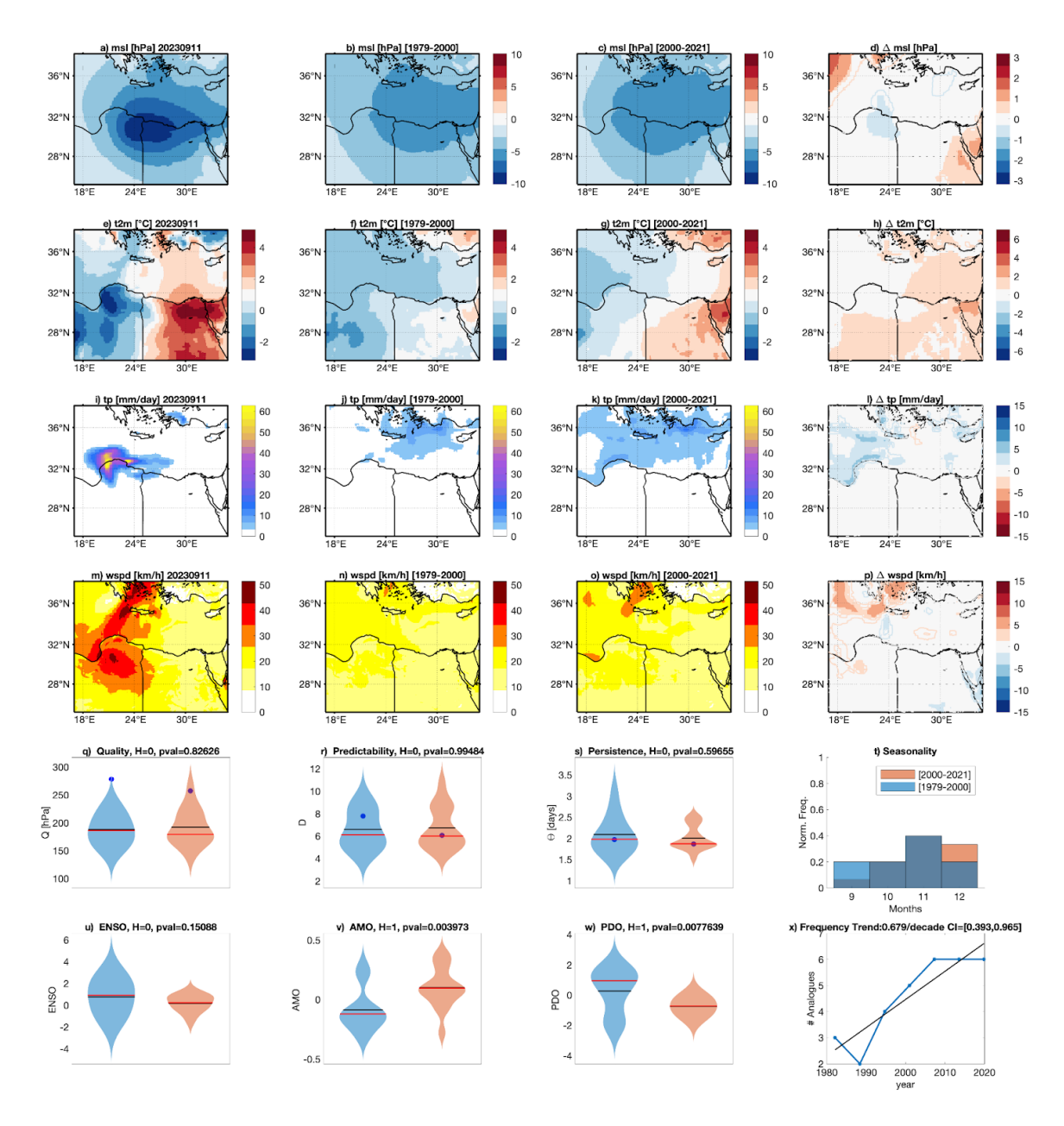
**Figure 10** Percentage of overlapping objects (in blue shading) among the ensemble prediction 1364 members for 24-hour accumulation (ending at the validity time) of extreme precipitation for different 1365 lead times valid on 6 September 2023, 00 UTC (left column panels) and 11 September 2023, 00 UTC 1366 (right column panels). Red contours show objects of extreme precipitation determined based on ERA5 1367 climatology (grey contours for MSLP isobars in ECMWF analysis).



**Figure 11** Six-hourly ensemble river discharge forecasts for the Peneus and Wadi Derna catchments 1374 compared to the "perfect forecast" benchmark (red line). The "perfect forecast" represents the 1375 initialization of each forecast for all time steps across the event, taken as a reference for evaluating 1376 forecast accuracy. With the observed timing of rising hydrograph limbs marked on 5 September, noon 1377 local time (09 UTC) for the Peneus River in Thessaly, and 10 September, 18:00 local time (16 UTC) 1378 for the Wadi Derna River. Grey stripes (tick marks) represent individual ensemble members from the 1379 EFAS model, driven by the 51 ensemble members of the ECMWF EPS. Overlapping tick marks 1380 darken, visually highlighting areas of member agreement (convergence). Forecast summary data are 1381 displayed as boxplots, where the box represents the interquartile range (IQR), the whiskers show the 1382 range of values within 1.5 times the IQR, and the horizontal black line inside the box indicates the 1383 median. The notches around the median show the 95% confidence interval.



**1387 Figure 12:** Analogues for 5 September 2023 and the region [15°E-33°E, 33°N-45°N] and the 1388 extended autumnsummer season SOND: average surface pressure anomaly (msl) (a), average 2-m 1389 temperature anomalies (t2m) (e), accumulated total precipitation (tp) (i), and average wind-speed 1390 (wspd) in the period of the event. Average of the surface pressure analogs found in the counterfactual 1391 [1979-2000] (b) and factual periods [2001-2022] (c), along with corresponding 2-m temperatures (f, 1392 g), accumulated precipitation (j, k), and wind speed (n, o). Changes between present and past analogs 1393 are presented for surface pressure  $\Delta$ mslslp (d), 2-m temperatures  $\Delta$ t2m (h), total precipitation  $\Delta$ tp (i), 1394 and wind speed  $\Delta$ wspd (p): color-filled shaded areas indicate significant anomalies obtained from the 1395 bootstrap procedure. Contours indicate non-significant changes; Violin plots for past (blue) and 1396 present (orange) periods for Quality Q analogs (q), Predictability Index D (r), Persistence Index  $\Theta$  (s), 1397 and distribution of analogs in each month (t). Violin plots for past (blue) and present (orange) periods 1398 for ENSO (u), AMO (v) and PDO (w). Number of the Analogues occurring in each subperiod (blue) 1399 and linear trend (black). A blue dot marks values for the peak day of the extreme event. Horizontal 1400 bars in panels (q,r,s,u,v,w) correspond to the mean (black) and median (red) of the distributions.



**1404 Figure 13:** As in Fig. 12, but for 10-11 September 2023, the region [17°E-35°E, 25°N-38°N] and the **1405** extended autumn season (SOND). **1406**